Axonal transport is required for a variety of neural functions including neurotransmitter synthesis, release and recycling (10). Motor neurons often have long axons that can be more than a meter in length in humans. For this reason, orderly function of the axonal transport mechanism should be particularly important in maintaining the structure and signal transmission at the terminals of motor axons. The transport process is carried out by two major families of motor proteins, i.e. kinesin super family for anterograde transport and the cytoplasimic dynein for retrograde transport (11). Defects in axonal transport have been reported as an early sign of motor neuron diseases including ALS (12). In mutant SOD1-Tg mice, anterograde transport of neurofilaments and tubulin is partially impaired long before disease onset, presumably due to an inhibition of certain transport systems (13,14). With respect to retrograde transport, mutations in the dynein heavy chain result in motor-selective dysfunction in mice (15). Moreover, mutation in $p150^{Glued}$, a subunit of dynactin (dynein activator), was identified in a family that developed a lower motor neuron-specific disease (16). These results strongly suggest a link between the integrity of the axonal transport mechanism with the function and survival of motor neurons.

We previously studied the intracellular localization of misfolded SOD1 species by subcellular fractionation of spinal cords from *SOD1*^{G93A}-Tg mice and found a significant accumulation of misfolded SOD1 species within the axon-enriched fraction at disease onset (17). From this result, together with previous reports, we hypothesized that misfolded SOD1 species may bind to proteins required for axonal transport and thereby inhibit normal function of the motor proteins. To prove this hypothesis, we screened axonal transport-related molecules in search for proteins that associate specifically to the misfolded SOD1 species and identified KAP3 as a misfolded SOD1-interacting protein. KAP3 is a component of the kinesin-2 motor complex mediating an axonal transport of choline acetyltransferase (ChAT) in *Drosophila* (18,19). By using an *in vitro* FALS modeling system that we developed, we showed that misfolded SOD1 inhibits axonal transport-dependent release of acetylcholine (ACh). Moreover, such impairment of ACh release could be rescued by the KAP3 overexpression. This evidence strongly suggests that the sequestering of KAP3 and the resultant inhibition of ChAT transport is a novel toxic property of mutant SOD1 proteins that inevitably leads to motor neuron-specific dysfunction.

RESULTS

Misfolded SOD1 species is accumulated in ventral white matter of spinal cords in *SOD1*^{G93A}-Tg mice prior to disease onset

We previously showed by using subcellular fractionation analysis that a considerable amount of misfolded SOD1 species is located in a fraction enriched in nucleus and certain kinds of cytoskeletal proteins (i.e. glial fibrilary acidic protein and neurofilament) in *SOD1*^{G93A}-Tg mice spinal cord prior to appearance of characteristic motor symptoms of ALS (17). To analyze more detailed subcellular localization of misfolded SOD1 in spinal motor neurons of *SOD1*^{G93A}-Tg mice, we divided the spinal cord into four subsegments by laser-assisted microdissection (LMD) (summarized in Fig. 1A) and used the lysate from each segment to detect SOD1 by immunoblot analysis. Since we observed that the *SOD1*^{G93A}-Tg mice we used in this study experienced disease onset around the age of 8 months (246.5 ± 5.8 days) and died around 9.5 months (288.5 ± 7.1 days, mean $\pm$ SEM, $n = 14$), we chose to collect samples from mice of 4, 7, 8 and 9 months of age. As expected, the majority of misfolded SOD1 species (high molecular-weight bands/smears immunoreactive for SOD1) was located in the ventral gray matter at 7 months of age, which is 1 month prior to disease onset (Fig. 1B and C). At this age, we also found that a significant amount of misfolded SOD1 species was located in ventral white matter, suggesting that misfolded SOD1 species are localized in motor neuron cell bodies and their axons. We further divided the ventral white matter segment into three subsegments and confirmed a localization of misfolded SOD1 species to a motor axon-enriched segment indicated by ChAT expression (Supplementary Material, Fig. S1). Together, these results suggest that a significant amount of misfolded SOD1 species is located not only in motor neuron cell bodies, but also in motor axons of *SOD1*^{G93A}-Tg mice prior to disease onset.

Misfolded SOD1 species associates with KAP3, a kinesin-2 component

Previous reports strongly suggest that impairment of the axonal transport mechanism is linked to degeneration of motor neurons (12). Localization of misfolded SOD1 species in motor axons of *SOD1*^{G93A}-Tg mice suggests that misfolded SOD1 species may affect the function of proteins required for axonal transport. Anterograde and retrograde axonal transports are mediated by different protein complexes, which are composed of a large variety of proteins. The kinesin super family for anterograde transport, for instance, is divided into six families (kinesin-1, 2, 3, 4, 13 and 14) consisting of 45 members in human and mouse, and they associate with appropriate cargos via adaptor molecules in most cases (11). To gain more insight into the relationship between misfolded SOD1 and individual components of the molecular motor protein complex, we compared sedimentation of misfolded SOD1 in linear density gradient centrifugation with that of representative molecules that compose motor complexes in motor axon lysate. We asked whether any of these motor complex components co-migrate with misfolded SOD1. Homogenates were prepared from the ventral white matter of *SOD1*^{G93A}-Tg mice at 8 months of age (disease onset) and *SOD1*^{WT}-Tg mice expressing human wild-type *sod1* gene (non-symptomatic control) and subjected to linear Nycodenz density gradient centrifugation. SOD1 immunoreactive bands showing expected molecular weight (representing normally folded SOD1) were observed in fractions nos 1–7 in mice of both genotypes. Misfolded SOD1 species, on the other hand, were found in fractions around no. 16 only in *SOD1*^{G93A}-Tg mice. We then examined migration profiles of 17 major components of the molecular motors from five kinesin families excluding kinesin-4 which is mostly expressed in juvenile brain,

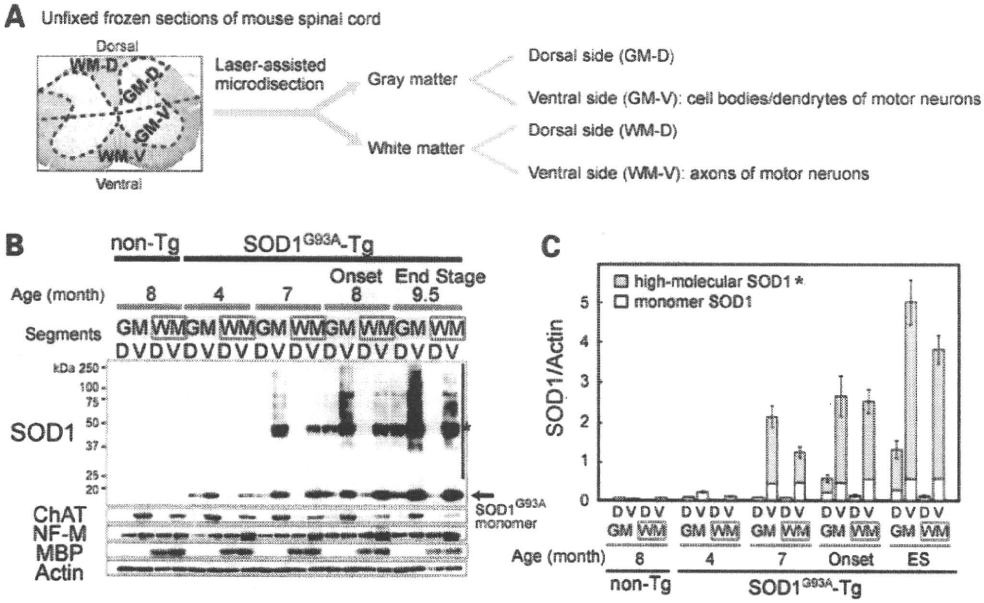

Figure 1. Misfolded SOD1 species were enriched in ventral white matter and ventral gray matter in spinal cord of *SOD1*^{G93A}-Tg mice prior to disease onset. (**A**) The procedure to divide and obtain subsegments of spinal cord is schematically shown. Unfixed frozen sections from L5 spinal cords were stained with 0.01% Toluidine blue and cut into four segments: dorsal white matter (WM-D), dorsal gray matter (GM-D), ventral white matter (WM-V) and ventral gray matter (GM-V) as indicated. (**B**) The presence of misfolded SOD1 species in the spinal cord subsegments obtained from 4, 7, 8 and 9.5 months old *SOD1*^{G93A}-Tg mice and 8 months old wild-type control (non-Tg) mice by immunoblot analysis is shown. Identity of the sample in each lane is indicated above the image. High molecular-weight bands/smears immunoreactive for SOD1 are the misfolded SOD1 species indicated by an asterisk. This misfolded SOD1 species appeared both in WM-V and GM-V of *SOD1*^{G93A}-Tg mice at 7 months. The same blot was analyzed for expression of ChAT (a motor neuron marker), neurofilament M (NF-M; a neuronal marker), MBP (a myelin marker) for controls. Actin served as a loading control. (**C**) The immunoreactivity of both monomeric (normally folded) and misfolded SOD1 that is shown in immunoblot analysis in (B) was quantified. The expression level of total SOD1 as well as monomeric and misfolded SOD1, in arbitrary units relative to actin expression is shown as a bar graph.

cytoplasmic dynein and dynactin. Among those molecules, KAP3, a subunit of the kinesin-2 motor complex, clearly co-migrated with misfolded SOD1 species around fraction no. 16 from *SOD1*^{G93A}-Tg mice (Fig. 2A, asterisks). In addition to KAP3, KIF3A and KIF3B, which are KAP3-binding partners, were weakly detected around fraction no. 16. We also observed p150^{Glued}, a dynactin subunit, co-migrated with misfolded SOD1 species. However, we did not proceed to a detailed analysis of this observation for now, because p50, another dynactin subunit (data not shown), or other dynein components such as Dynein intermediate chain (Dynein IC in Fig. 2A) did not co-migrate with misfolded SOD1 species. To confirm this association of KAP3 with misfolded SOD1, we performed immunoprecipitation analysis using the fraction nos 16 and 7. KAP3 was identified in anti-SOD1 immunoprecipitates obtained from fraction no. 16 containing misfolded SOD1 species but not in the fraction from no. 7 (Fig. 2B). In reciprocal immunoprecipitation, we found misfolded SOD1 in anti-KAP3 immunoprecipitates only in fraction no. 16. CRMP-2 (collapsin response mediator protein-2), a KAP3 counterpart for kinesin-1 motor complex, did not associate with misfolded SOD1. KAP3 seems to be associated with misfolded SOD1 species at least 2 months before disease onset, since the misfolded SOD1 species was detected in the immunoprecipitate with anti-KAP3 antibody from the extracts of 6-month-old *SOD1*^{G93A}-Tg spinal cords (Fig. 2C). Furthermore, we examined immunohistochemical localization of SOD1 and KAP3 on spinal cord sections of *SOD1*^{G93A}-Tg mice at 9 months of age (end stage). We found that protein aggregates in the remaining spinal motor neurons, immunoreactive for KAP3 were also positive for SOD1 (Fig. 2D, upper panel). The KAP3-positive aggregates also contained ubiquitin immunoreactivity, suggesting that the aggregates are cellular inclusion bodies (Fig. 2D, lower panel). These results suggest that misfolded SOD1 species specifically binds to KAP3 in motor axons of *SOD1*^{G93A}-Tg mice and that this association starts prior to the onset of motor symptoms.

Axonal transport of ChAT was significantly impaired in spinal motor neurons preceding disease onset in SOD1^{G93A}-Tg mice

Kinesin-2 is a ubiquitously and abundantly expressed molecular motor complex, which consists of KAP3 and KIF3A, together with either KIF3B or KIF3C (20). The motor domain consisting of KIF3A along with either KIF3B or KIF3C translocates along microtubules with hydrolyzing ATP, and KAP3 determines the specific cargo to be transported. Recent work using *Drosophila* ganglionic cells showed that kinesin-2 is involved in the transport of ChAT and ACh esterase (AChE) (18). Although both of the enzymes are essential for an efficient supply of ACh to the nerve terminals of spinal motor neurons, the amount of

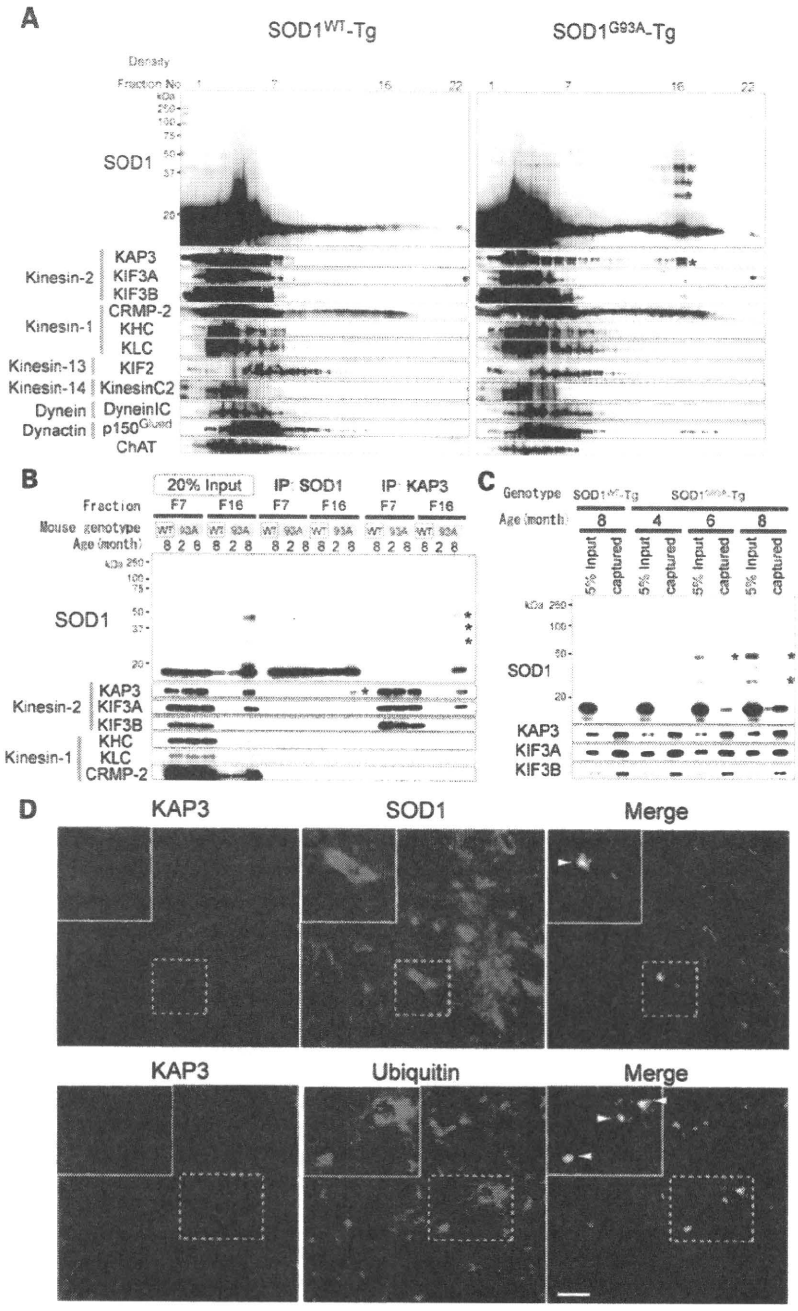

Figure 2. Misfolded SOD1 species in ventral white matter of spinal cords specifically associates with KAP3. (**A**) Fractions obtained from Nycodenz density gradient centrifugation of ventral white matter of 8-month-old *SOD1*^{WT}-Tg and *SOD1*^{G93A}-Tg spinal cords were analyzed for the presence of indicated proteins (SOD1 and individual components of kinesin and dynein motor complexes) by immunoblot analysis. Each lane (left to right) represents an aliquot collected from the top. Note that misfolded SOD1 species (indicated by asterisks) migrated around fraction no. 16 in *SOD1*^{G93A}-Tg spinal cords, where KAP3 co-migrated. (**B**) Immunoprecipitates of anti-SOD1 and KAP3 antibodies (indicated as 'IP:SOD1' or 'IP:KAP3') from Nycodenz density gradient centrifugation fractions 7 and 16 (F7, F16) of *SOD1*^{G93A}-Tg mouse spinal cords prepared above were analyzed for the presence of indicated proteins by immunoblot analysis. Also shown is an immunoblot of samples F7 and F16 (20% of the amount used for immunoprecipitation) examined for expression of the same set of proteins. Note that misfolded SOD1–KAP3 association was detected from F16 but not from F7. (**C**) Immunoprecipitates of anti-KAP3 antibody from whole spinal cord extracts of 4-, 6- and 8-month-old *SOD1*^{G93A}-Tg mice and 8-month-old *SOD1*^{WT}-Tg mice were analyzed for the presence of misfolded SOD1 by immunoblot. KIF3A and KIF3B, which are kinesin-2 components, served as controls for immunoprecipitation. Note that misfolded SOD1 species (asterisks) were captured by anti-KAP3 antibody in 6- and 8-month-old *SOD1*^{G93A}-Tg extracts. (**D**) Representative photographs of immunohistochemical co-localization of KAP3 and SOD1 (upper panel), and KAP3 and ubiquitin (lower panel) in a 9-month-old *SOD1*^{G93A}-Tg mouse spinal cord. Insets show higher magnification images of boxed area. Arrowheads indicate aggregate-like structures within motor neuron cell bodies, which were positive for both KAP3 and SOD1 (upper panel) and KAP3 and ubiquitin (lower panel). Scale bars=50 μm.

ChAT supplied is more critical for the overall production of ACh (21). Therefore, to examine the impact of misfolded SOD1–KAP3 association on the function of motor neurons in *SOD1*^{G93A}-Tg mice during the disease progression, we decided to analyze the transport of ChAT in motor neurons. To achieve this, we obtained motor–cargo protein complexes using a previously described method from ventral roots of the caudal spinal cord, which represent motor axons just extended from the spinal cords and examined the presence of ChAT by immunoblot analysis. We found that a significantly lower level of ChAT was present in cauda equina of *SOD1*^{G93A}-Tg mice compared with those of *SOD1*^{WT}-Tg at 7 months of age or later (Fig. 3A). Furthermore, kinesin-2 motor components, KAP3, KIF3A and KIF3B, all showed a similar decrease in expression during the disease progression in cauda equina of *SOD1*^{G93A}-Tg mice. On the other hand, KHC (kinesin heavy chain), KLC (kinesin light chain) (kinesin-1 components) and Rab3 (a synaptic vesicle-associated protein transported by KIF1A) were consistently expressed during the disease progression. Decreased ChAT transport in pre-symptomatic *SOD1*^{G93A}-Tg mouse sciatic nerve was also demonstrated by a ligation assay (Supplementary Material, Fig. S2A). These results suggest that the amount of ChAT transported by the kinesin-2 complex significantly decreases in motor axons of *SOD1*^{G93A}-Tg mice prior to disease onset.

The results presented in Figure 2A show that ChAT does not co-migrate with the misfolded SOD1–KAP3 complex, suggesting that KAP3 does not bind to ChAT and misfolded SOD1 at the same time. Decreased amounts of ChAT and kinesin-2 motor complex within the axons of motor neurons in *SOD1*^{G93A}-Tg mice, together with Figure 2A data, suggest that the misfolded SOD1 species may inhibit kinesin-2-mediated ChAT transportation by trapping the kinesin-2 motor complex in the motor neuron cell body and the surrounding areas. For a better understanding of the misfolded SOD1 species behavior in motor axons of *SOD1*^{G93A}-Tg mice, we compared the migration profile in a sucrose density gradient centrifugation of kinesin motor components and ChAT with that of SOD1, by using the axonal motor-cargo protein complexes prepared above as a sample. We found that a small amount of misfolded SOD1 species are present in axonal motor–cargo protein complexes and co-migrate with a small fraction of KAP3, KIF3A (Fig. 3B) and KIF3B, although the detection of KIF3B requires very long exposure (data not shown). We also found that ChAT co-immunoprecipitates with KAP3 in fractions where KAP3 and kinesin-2 components co-migrated. (Supplementary Material, Fig. S2B). These results suggest that misfolded SOD1 species not only trap the kinesin-2 motor complex via association with KAP3 in and around the cell bodies but some of the misfolded SOD1 is also transported to axons in stead of normal cargos such as ChAT.

NG108-15 cells serve as an *in vitro* model for FALS

We showed a clear correlation between the association of misfolded SOD1 with KAP3 and the inhibition of ChAT transport within *SOD1*^{G93A}-Tg mouse motor axons. To examine the causal relationship between these two phenomena in detail, we developed a novel cell culture model for FALS, in which

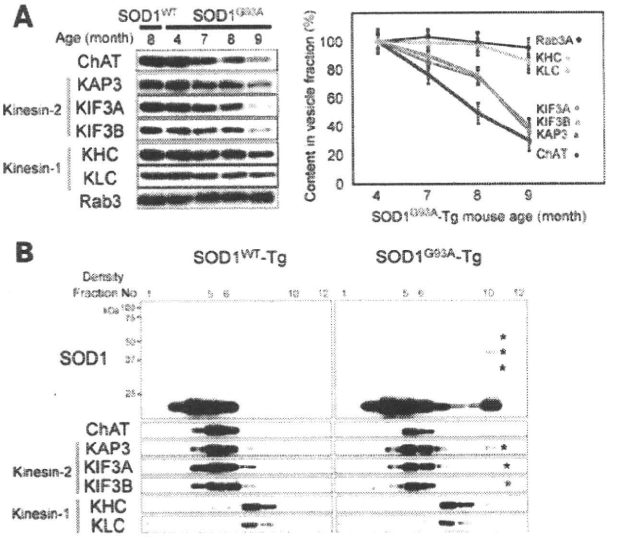

Figure 3. Axonal transport of ChAT was selectively impaired in spinal motor neurons preceding disease onset in SOD1^{G93A}-Tg mice. (**A**) Axonal transport components obtained from ventral roots from caudal spinal cords of *SOD1*^{WT}-Tg and *SOD1*^{G93A}-Tg mice at indicated ages were analyzed for the presence of indicated proteins by immunoblot analysis (left panel). The expression level of each molecule examined for *SOD1*^{G93A}-Tg mice is shown as a percentage of the level at 4 months of age (right panel). Note that the decrease in detection levels of ChAT and kinesin-2 components (KAP3, KIF3A and KIF3B) in *SOD1*^{G93A}-Tg mice became apparent at 7 months of age, 1 month before disease onset. (**B**) Fractions obtained from a sucrose density gradient centrifugation of axonal transported components from 8-month-old mice were analyzed for the presence of indicated proteins (SOD1 and individual components of kinesin motor complexes) by immunoblot analysis. Each lane (left to right) represents an aliquot collected from the top. Note that only kinesin-2 components co-migrated with misfolded SOD1 species (indicated by asterisks on the blots).

cells show cholinergic neuron-like properties—ChAT is transported within axon-like processes, ACh is released by depolarization and mutant SOD1 is misfolded/aggregated. For this purpose, we employed NG108-15 cells, which are of neuron/glia origin and known to differentiate into a cholinergic neuron-like phenotype (22,23). We first cloned a single cell-derived subline of NG108-15 cells, which we termed PNG3 (Purified NG108-15 cell-3), that showed highest expression of ChAT upon differentiation with dibutyryl cAMP and dexamethasone (data not shown). We observed that expression of ChAT and synaptophysin (an integral membrane protein found on synaptic vesicles) reaches the maximal level at ~72 h after the stimulation (Fig. 4A). By immunocytochemistry, we found that expression of ChAT and KAP3 were predominantly detected within the extended PNG3 processes in 72 h after the stimulation (Fig. 4B) as other kinesin-2 subunits (data not shown). From these observations, we decided to use PNG3 cells as a model for cholinergic neurons at day 3 after initiating differentiation for all the following experiments.

In order to use PNG3 cells as a cell line model for FALS, misfolding/aggregate formation by mutant SOD1 overexpression needs to be observed. Oxidative stress tends to cause mutant SOD1 proteins misfold and form aggregates (4). Experimentally, mutant SOD1 aggregate formation can be observed and facilitated by inhibiting proteasomal activity (24,25).

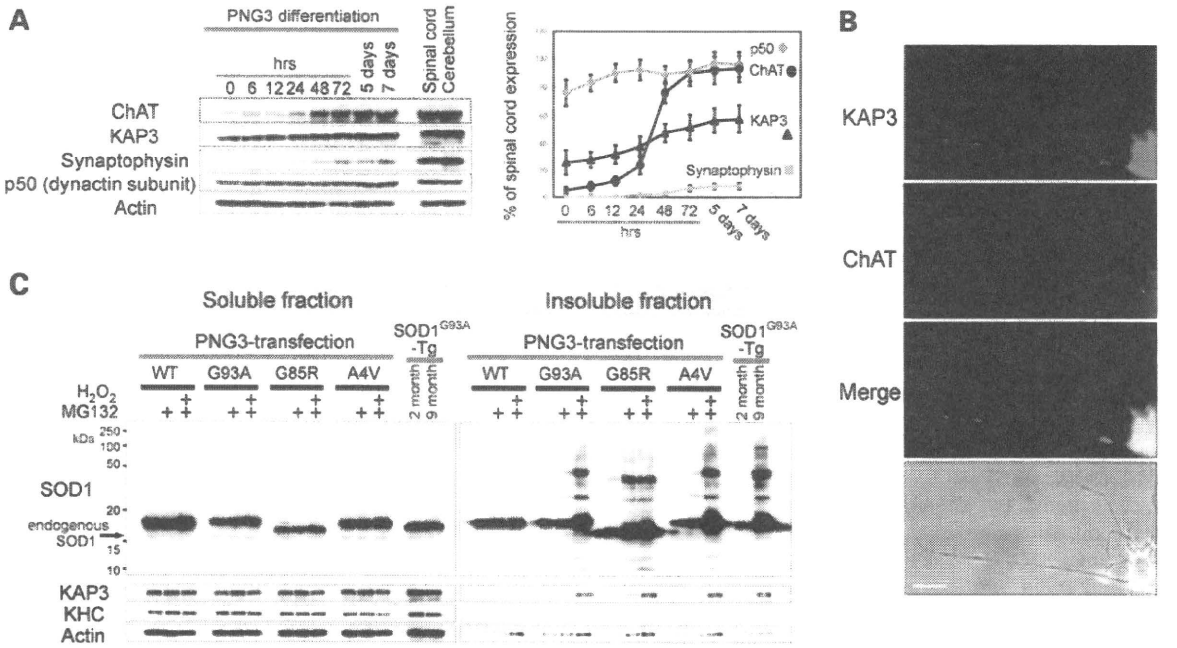

Figure 4. PNG3 cells served as an *in vitro* model system for studying mutant SOD1 toxicity on cholinergic neurons. (**A**) Expression of indicated proteins in PNG3 cells during cholinergic neuron-like differentiation was examined by immunoblot analysis. PNG3 cells were lysed at indicated times after induction of differentiation by dibutyryl cAMP and dexamethasone. Representative images of immunoblots (left panel) and quantitative analysis of the blots (right panel) are shown. Expression level is normalized to actin and relative to the level of normal spinal cord at each time point for each molecule. (**B**) Representative photographs of ChAT and KAP3 expression in differentiated PNG3 cell bodies and processes detected by immunocytochemistry are shown. Scale bar=25 μm. (**C**) Generation of misfolded SOD1 species in PNG3 cells overexpressing FLAG-tagged SOD1 bearing WT, G93A, G85R or A4V mutation was evaluated by immunoblot analysis. The transfected PNG3 cells were either untreated, treated by MG132 or treated by MG132 followed by H_2O_2 (as indicated above the images). One perecnt Triton X-100-soluble and -insoluble fractions were separately analyzed for SOD1-FLAG, KAP3, KHC and actin (for loading control). Spinal cords of 2- and 9-month-old *SOD1*^{G93A}-Tg mice were also subjected for the same set of analysis for comparison.

Therefore, we used a combined condition of increased oxidative stress plus decreased proteasomal activity to induce SOD1 misfolding and to enhance an accumulation of those misfolded SOD1 species in differentiated PNG3 cells overexpressing mutant SOD1. We transfected PNG3 cells with previously well-studied G93A, G85R and A4V mutations and wild-type control of human SOD1 for overexpression (3). Misfolded SOD1 species was detected in1% Triton X-100 insoluble fractions of lysates derived from all three types of FALS-linked SOD1 mutant transfectants but not in wild-type SOD1-overexpressing cells (Fig. 4C). We also found that SOD1 protein bearing the G85R mutation became misfolded without increasing oxidative stress, showing the previously reported unstable nature of this mutant protein (24). These results suggest that mutant SOD1 can form misfolded and/or aggregated molecules in differentiated PNG3 cells, very similar to what is seen in SOD1^{G93A}-Tg mice by pathological stresses.

For the analysis of pathological significance of misfolded SOD1–KAP3 association in this PNG3 cell model system, we next asked whether association of KAP3 with misfolded SOD1 is observed in this model just as we saw in the *SOD1*^{G93A}-Tg mice. To prove the association of KAP3 with misfolded SOD1 directly, we performed immunoprecipitation experiments using lysates of PNG3 cells transfected with either wild-type or mutant SOD1, and then treated with hydrogen peroxide to induce the mutant SOD1 misfolding. We found that anti-KAP3 immunoprecipitates contained misfolded SOD1 species, and the antibody against mutant SOD1-Flag immunoprecipitated misfolded SOD1 together with KAP3 (Fig. 5A). To visualize the misfolded SOD1-KAP3 association in PNG3 cells, we performed immunocytochemical analysis for localization of KAP3 and mutant SOD1. We found mutant SOD1-immunoreactive aggregates were prominent in cell bodies as well as the processes of MG132-treated differentiated PNG3 cells expressing G85R SOD1, and those aggregates were also positive for KAP3 (Fig. 5B and C). These observations together suggest that the cellular FALS model that we developed here using PNG3 cells recapitulates the association of KAP3 and misfolded SOD1 observed in *SOD1*^{G93A}-Tg mice and therefore is suitable to analyze the pathological impact of the misfolded SOD1-KAP3 association on motor neurons.

Microtubule-dependent fraction of depolarization-induced ACh release from PNG3 cells requires KAP3

In *Drosophila* neurons, the kinesin-2 motor complex is responsible for anterograde axonal transport of ChAT (18,19). To examine whether the same is true in mammals, we first developed an assay model to detect a depolarization-induced microtubule-dependent release of ACh as a result of ChAT transport. Differentiated PNG3 cells were metabolically

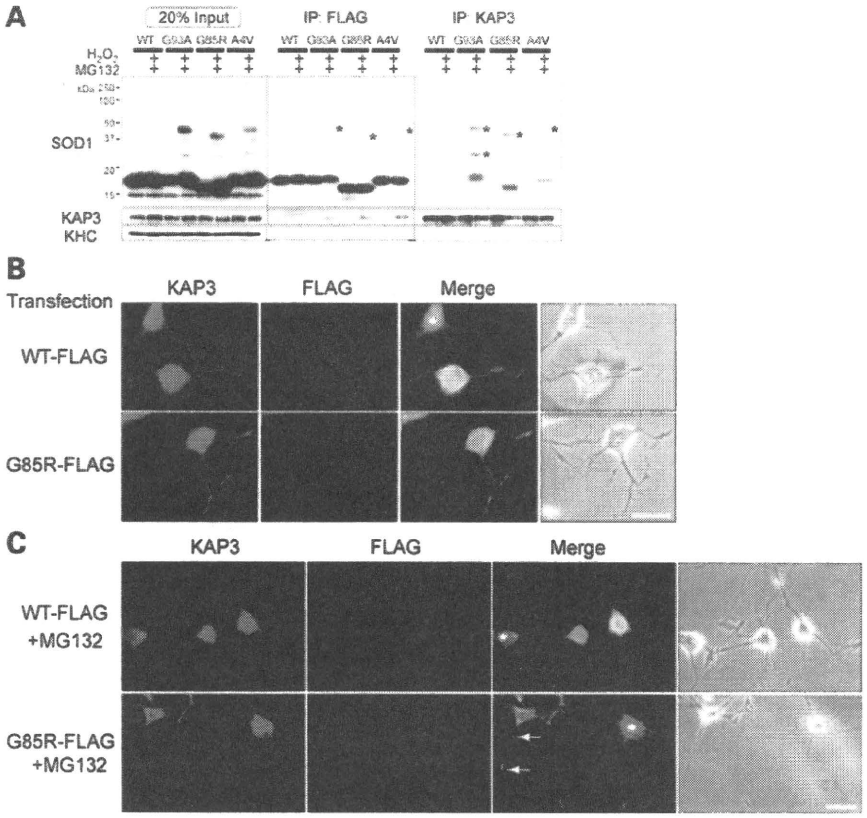

Figure 5. KAP3 associates with misfolded SOD1 species in differentiated PNG3 cells. (**A**) Immunoprecipitates of anti-FLAG and KAP3 antibodies (labeled as 'IP:FLAG' or 'IP:KAP3') from lysates of PNG3 cells transfected with expression plasmids for wild-type SOD1 or SOD1 with G93A, G85R or A4V mutation with or without induction of misfolding by MG132/H_2O_2 were analyzed for the presence of indicated proteins by immunoblot analysis. Immunoblot of lysates used for immunoprecipitation (20% of the amount) of the expression of the same set of proteins is also shown. Note that misfolded SOD1–KAP3 association was detected in all three mutant SOD1 transfectants (indicated by asterisks). (**B** and **C**) Photographs of KAP3 and FLAG-tagged SOD1 in differentiated PNG3 cells transfected with either FLAG-tagged wild-type SOD1 or SOD1 bearing a G85R mutation before and after MG132 treatment are shown in (B) and (C), respectively. Phase contrast images are also shown to the right of each set. Asterisks indicate untransfected cells. Note that prominent aggregate formation is only in the mutant SOD1-expressing cells and processes after MG132 treatment. Scale bars=25 μm.

labeled with [^{3}H]choline, and depolarization-induced [^{3}H] ACh release was measured. We observed that PNG3 cells released [^{3}H]ACh in a KCl dose-dependent manner (Fig. 6A). To distinguish 'nerve terminal' ACh release from exocytosis at other locations, we examined ACh release with and without colchicine, a microtubule destabilizing reagent that inhibits axonal transport (18). From ACh release experiments with different trial amounts of colchicine, we decided to use colchicine at 2.5 μM for the best differentiation of microtubule-dependent release representing the release from the terminal of differentiated PNG3 cellular processes. Treating the cells with this concentration converted nearly 20% of the tubulin from filamentous to free form in PNG3 cells (Supplementary Material, Fig. S3A). Then to analyze the involvement of KAP3/kinesin-2 in ChAT transport in the mammalian neuron using this assay system, we examined the effect of KAP3 mRNA down-regulation in differentiated PNG3 cells. Although NG108-15 cells are mouse–rat hybrid, transfection of siRNA for mouse KAP3 in PNG3 cells decreased the KAP3 protein level to ~15% after 2 days (Supplementary Material, Fig. S3B). We found that siRNA-mediated down-regulation of KAP3 significantly reduced the microtubule-dependent fraction of ACh release from PNG3 cells (Fig. 6B). This reduction in ACh release was rescued by the co-transfection of full-length human KAP3 which is not affected by the mouse siRNA we used. However, the ACh release was not rescued by the human KAP3 lacking C-terminal sequence (513–792 amino acids), which is required for the interaction with KIF3A/B (26). These results suggest that KAP3 is required for ChAT transport along microtubules and the subsequent release of ACh from nerve terminals in mammalian neurons.

As described above, we observed decreased ChAT axonal transport in *SOD1*^{G93A}-Tg mice. To examine whether misfolded SOD1 inhibits ChAT transport also in this FALS model system in culture, we measured microtubule-dependent ACh release from differentiated PNG3 cells after induced production of misfolded SOD1 species (procedure is summarized in Fig. 6C). We found that induction of SOD1 misfolding by MG132 treatment resulted in a significant decrease of microtubule-dependent ACh release from mutant SOD1-expressing PNG3, but not from wild-type SOD1-expressing cells

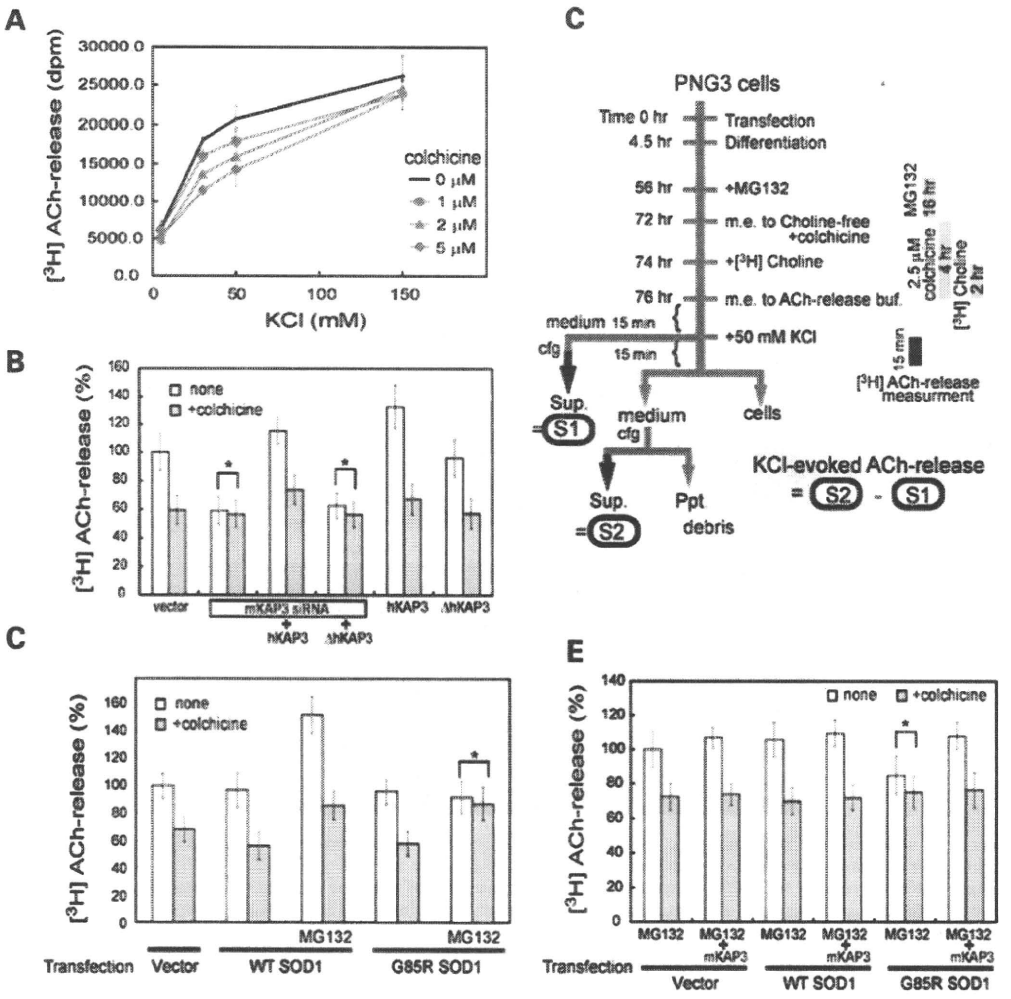

Figure 6. Microtubule-dependent fraction of depolarization-induced ACh release from PNG3 cells requires KAP3. (**A**) Differentiated PNG3 cells, metabolically labeled with [^{3}H]choline, were depolarized by increased KCl in the medium for 15 min. The radioactivity was released into the medium representing [^{3}H]ACh and was measured for different concentrations of KCl and colchicine, as indicated. (**B**) Depolarization-induced [^{3}H]ACh release from differentiated PNG3 cells transfected with vector only, siRNA for mouse KAP3 (mKAP3) or siRNA for mKAP3 together with expression plasmid for either human KAP3 (hKAP3) or hKAP3 lacking C-terminal 223 amino acids (ΔhKAP3), expression plasmid for hKAP3 only or expression plasmid for ΔhKAP3 was determined with or without colchicine treatment. Radioactivity is shown as a percentage to that from vector-transfected, colchicine-untreated cells. The asterisk indicates non-significant differences calculated as $P > 0.05$. Note that KAP3 down-regulation inhibited microtubule-dependent ACh release. (**C**) Summarized time schedule for [^{3}H]ACh-release measurement in differentiated PNG3 cells with and without SOD1 misfolding/aggregation. KCl-evoked release of ACh was calculated by subtracting the radioactivity in S1 (medium before KCl addition) from that in S2 (medium after KCl addition). (**D**) Depolarization-induced [^{3}H]ACh release from differentiated PNG3 cells transfected with vector only, expression plasmid for wild-type SOD1 or G85RSOD1 was determined with or without MG132 treatment. Microtubule-dependent and -independent fractions of release were measured for each condition analyzed. Radioactivity is shown as percentage to that from vector-transfected, colchicine-untreated cells. Note that ACh release from mutant SOD1-transfected cells was reduced in response to MG132 treatment, while overexpression of mutant SOD1 *per se* did not affect choline incorporation into cells (Supplementary Material, Fig. S4C). The asterisk indicates non-significant difference calculated as $P > 0.05$. (**E**) Depolarization-induced [^{3}H]ACh release from differentiated PNG3 cells transfected with vector only, expression plasmid for wild-type SOD1 or G85RSOD1, with or without co-transfection of mKAP3 expression plasmid, was determined after MG132 treatment. Microtubule-dependent and -independent fractions of release were measured for each condition analyzed. Radioactivity is shown as a percentage of that from vector-transfected, colchicine-untreated cells. Note that the reduction in ACh release observed in mutant SOD1-transfected cells in response to MG132 treatment was normalized by mKAP3 expression. The asterisk indicates non-significant difference calculated as $P > 0.05$.

(Fig. 6D, asterisk). MG132 treatment itself resulted in up-regulation of both microtubule-dependent and -independent ACh release (Fig. 6D and Supplementary Material, Fig. S4A). However, this MG132-induced increase in ACh release was presumably caused by increased expression levels of proteins necessary for ACh synthesis/release and was independent from the misfolded SOD1-induced effect (Supplementary Material, Figs S4B and C). These results suggest that misfolded SOD1 inhibits ChAT transport in this FALS model system in culture as well.

The observations in *SOD1*^{G93A}-Tg mice, as well as in the cellular FALS model system that we described, further

suggest that misfolded SOD1 causes a reduction or depletion of the functional kinesin-2 complex via its association with KAP3. This raises the possibility that misfolded SOD1-induced reduction in ChAT transport may be normalized by supplementing motor neurons with KAP3. To prove this hypothesis using the FALS culture model system, we examined microtubule-dependent ACh release from differentiated PNG3 cells overexpressing wild-type or mutant SOD1 together with KAP3. Overexpression of KAP3 did not change ACh release from MG132-treated PNG cells transfected with empty vector or wild-type SOD1. However, overexpression of KAP3 was able to normalize the ACh release reduction under the condition that causes mutant SOD1 misfolding (Fig. 6E). These results strongly suggest that misfolded SOD1-induced reduction in ChAT transport and ACh release is mediated by a reduction in functional KAP3 molecule because of its association with misfolded SOD1. These results may also suggest that the normalization of functional KAP3 level in motor neurons could have a therapeutic effect on FALS pathogenesis.

KAP3 was co-localized with mutant SOD1 aggregates within LBHI in spinal motor neurons from human FALS patients

As described, we performed analysis of the misfolded SOD1-induced reduction of ChAT transport in cultured cells in cultured cells as well as in a mouse model. To gain insight into the significance of this mechanism in human FALS, we performed immunohistochemistry on spinal cord sections of human SOD1-linked FALS cases to examine co-localization of KAP3 and SOD1. The neuropathological phenotypes of four patients we analyzed, who were members of two different families (27–29), are summarized in a table in Figure 7. These patients often developed Lewy-body-like hyaline inclusions (LBHIs), which are protein aggregates containing mutant/wild-type SOD1 and one of the most characteristic cytopathological changes in the spinal motor neurons of mutant *sod1*-linked FALS (28). Immunohistochemical analysis revealed that most of the LBHIs in the spinal motor neurons were positive for both KAP3 and SOD1 (arrowheads in Fig. 7). We confirmed that the KAP3 signal in LBHIs was not present when the anti-KAP3 antibody was pre-incubated with an excess of the synthetic KAP3 antigen peptides (data not shown). These observations demonstrated that KAP3–SOD1 interaction and subsequent co-aggregation frequently occurs in human SOD1-linked FALS cases.

DISCUSSION

In this paper, we presented a novel pathological mechanism by which misfolded SOD1 may cause neuronal dysfunction in FALS. A significant proportion of misfolded SOD1 is located within motor axons prior to disease onset in *SOD1*^{G93A}-Tg FALS model mice. We showed that misfolded SOD1 species selectively binds to KAP3 (Fig. 2B and C) and that this binding may be a cause for the reduction in functional KAP3 molecule required for kinesin-2-dependent

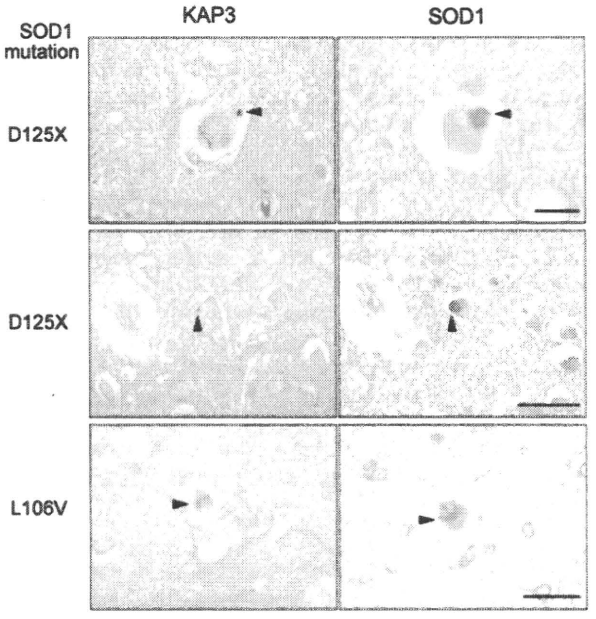

Neuropathological findings in autopsied patients with FALS examined.

SOD1 mutation	Number of patients	Neuronal inclusion	SOD1 aggregation	Bunina body	Corticospinal tract involvement	Posterior column involvement
D125X	2	LBHI	+	-	+	+
L106V	2	LBHI	+	-	+	+

+: present, -: absent, LBHI: Lewy-body-like hyaline inclusion

Figure 7. KAP3 was co-localized with SOD1 aggregates within LBHI in spinal motor neurons from human FALS cases. Consecutive sections of LBHI-containing spinal motor neurons from FALS patients possessing *sod1* mutations were immunostained with anti-KAP3 and anti-SOD1 antibodies. The clinicopathological characteristics of the FALS patients are summarized in the table. D125X mutation is a deletion of two nucleotides at codon 126 that results in the truncation of five residues downstream. Co-localization of KAP3 and SOD1 within the LBHI is evident (arrowheads). The images are representative of 30 LBHIs observed in each case, all of which showed co-localization of SOD1 and KAP3. Scale bars=25 μm for the images of top row, 50 μm in others.

transport within motor axons (Fig. 3A and B). The kinesin-2 motor complex is particularly important, because it is required for ChAT transport (19). Decreased ChAT expression and resultant decrease in ACh release from motor nerve ends can lead to dysfunction of motor synapses at axon terminals (30,31). By employing a newly developed cell culture model of FALS, we showed that ACh release from nerve terminals was decreased presumably due to a reduction in ChAT transport resulting from KAP3 sequestration by misfolded SOD1 species (Figs 5A and C and 6D). The pathological mechanism we propose from our data is schematized in Figure 8.

ALS-like motor neuron pathology is observed in transgenic mice expressing C-terminal truncated SOD1 (L126Z), in which the mutant SOD1 expression was not clearly observed in sciatic nerve (32). This suggests that KAP3-misfolded SOD1 association is formed mostly in motor neuron cell bodies. Indeed, we detected KAP3-misfolded SOD1 associ-

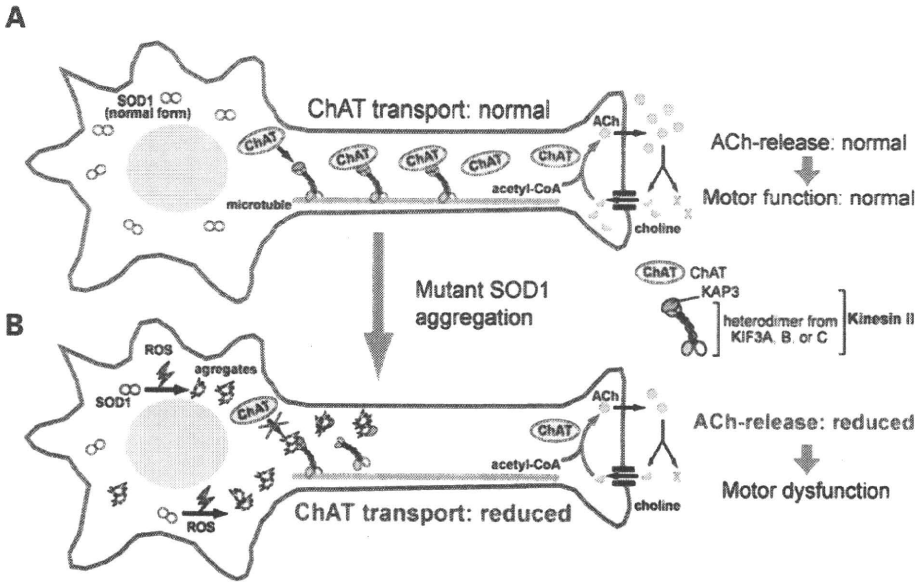

Figure 8. A schematic diagram for a mutant SOD1 toxicity and impairment of axonal transport of ChAT. In healthy motor neurons (**A**), ChAT is continuously transported by kinesin-2 motor, comprising KIF3A, KIF3B/C and KAP3, toward the neuromuscular junction where ACh functions as a neurotransmitter. ACh is released into the synaptic cleft upon stimulation and rapidly degraded into choline and acetic acid by AChE. Choline is taken up into the nerve terminal by choline transporters and then ChAT synthesizes ACh from choline and acetyl-CoA. The reaction catalized by ChAT is the rate-limiting step for ACh supply to the nerve terminals. In motor neurons expressing mutant SOD1 (**B**), mutant SOD1 proteins were converted into misfolded forms as a result of increased ROS generation and/or reduced proteasomal activity. Certain misfolded species preferentially binds to KAP3 and inhibit the binding of ChAT to KAP3, thereby causing a decrease in ChAT transport. This decrease in ChAT in the nerve terminals can constitute a mechanism that causes motor dysfunction.

ation in spinal cords (Fig. 2C) and ventral white matter (Fig. 2A and B) of *SOD1*^{G93A}-Tg mice prior to disease onset, but could not detect it in distal sciatic nerve even at the end-stage (data not shown). These findings suggest that, even if misfolded SOD1 associates with molecular motors, it cannot travel for a long distance, presumably because it is not a physiological cargo.

We suspect that misfolded SOD1–KAP3 association is one of the early events in FALS pathogenesis. Evidence to support this possibility is that the SOD1–KAP3 association becomes detectable around 6 months of age in *SOD1*^{G93A}-Tg mice, 2 months earlier than disease onset (Fig. 2C), suggesting that the SOD1–KAP3 association constitutes an early event in FALS motor neurons. Also, our immunoprecipitation/immunoblot analysis shows that SOD1–KAP3 association always detected relatively low molecular-weight misfolded SOD1 (−50 kDa) among all of the misfolded products ranging up to hundreds of kilodaltons in size (Figs 2B and C and 5A). The preferential association of KAP3 for low molecular-weight species but not with large precipitates suggests that SOD1–KAP3 association accounts for a fraction of the initial events in FALS pathogenesis. Previous reports on selective increase in KAP3 transcription in lumbar spinal cords from *SOD1*^{G86R}-Tg mice as an early event prior to disease onset (33) also supports our hypothesis, as the increase may be regarded as compensatory to the KAP3 sequestration by SOD1–KAP3 association.

Previous reports show that crossing mutant SOD1-Tg mice with dynein heavy chain mutant mice (*loa* or *cra*) delays the disease onset and extends survival (34,35). This result is surprising because mutations in dynein heavy chain, a subunit of dynein motor complex, or p150^{Glued}, a subunit of dynactin (dynein activator) cause dysfunction and degeneration of spinal motor neurons (15,16). This suggests a possible mechanistic link between impaired axonal transport in mutant *SOD1*-Tg mice and that in dynein heavy chain mutant mice. Here we demonstrated that KAP3 sequestration by misfolded SOD1 is a mechanism for selective inhibition of axonal transport observed in mutant SOD1-Tg mice. Previous reports on melanophore transport in *Xenopus* melanosomes showed that dynactin serves as an activator of kinesin-2 via direct binding of p150^{Glued} to KAP3 and regulates the intracellular direction of melanosome transport by binding to either dynein (retrograde) or KAP3 (anterograde) (36). Dynein and KAP3 share the same binding site on p150^{Glued}, and so p150^{Glued} binds to only one of them at a time and thereby activates transport in only one direction. If a similar regulation by dynactin plays a role in mammalian neurons, *loa* and *cra* mutations may increase the chance of p150^{Glued} to bind to KAP3, because those mutations promote subunit disassembly and increase dynein-unbound dynactin (15). By this mechanism, dynein heavy chain mutations may result in normalizing kinesin-2-mediated transport of ChAT inhibited by the misfolded SOD1 species. Indeed, in our analysis of ventral white matter in *SOD1*^{G93A}-Tg mice using Nycodenz density gradient centrifugation, a small fraction of p150^{Glued} co-migrated with misfolded SOD1 species and KAP3 (Fig. 2A). This population of p150^{Glued} also co-precipitated with KAP3 (data not shown). This result may reflect an involvement of p150^{Glued} in KAP3/SOD1 misfolding and aggregation through its interaction with KAP3.

A recent study provides an interesting evidence that transcription of all members of the KIF3 family selectively decreases in motor cortex of sporadic ALS patients among 13 kinds of kinesin and kinesin-related proteins (37). Impaired neuromuscular transmission was detected in early sporadic ALS patients (38), and a reduced supply of releasable ACh was thought to be the primary cause for the degeneration of motor terminal in a dog model of hereditary spinal muscular atrophy (30,39). It is possible that kinesin-2 dysfunction and subsequent inhibition of ChAT transport might be one of the common pathways leading to motor neuron-specific dysfunction in both sporadic and familial ALS cases.

The cargos and adaptor molecules for kinesin-2 have not been well studied. Small GTP-binding protein dissociation factor SmgGDS (40), fodrin (41), a tumor suppressor adenomatous polyposis coli (42), N-cadherin (43), ChAT and AChE (18) have been reported as molecules that bind to KAP3. Our finding that misfolded SOD1 species sequesters KAP3 raises a possibility that the transport of these molecules may also be impaired in mutant SOD1-related FALS, together with the reduced ChAT transport. Indeed, we observed a slight decrease in N-cadherin transport in motor axons from presymptomatic *SOD1*^{G93A}-Tg mice (Supplementary Material, Fig. S5). The expression and function of those molecules within motor neurons need to be studied to elucidate the entire mechanism.

MATERIALS AND METHODS

All the data in Figures 1–6 are a representative of three mice per group or three independent experiments. Statistical significance was assessed by ANOVA followed by Fisher's test. Error bars in graphs represent standard deviations. Signals in immunoblots were detected using ECL (GE Healthcare) and quantified with NIH image software (1.61J).

Reagents

All four types (WT, G93A, G85R and A4V) of FLAG-tagged human SOD1 cDNA at the C terminus were cloned into pcDNA3 (44). Full-length mouse (Image clone ID: 5698182) and human (4829354) KAP3 were purchased from Image clone bank and cloned into pcDNA3 and pCMV-Tag1, respectively. The integrity of each clone was verified by nucleotide sequence analysis. The siRNA designed for silencing mouse KAP3 (M-047278-00-0010) was purchased from Dharmacon Research. Primary antibodies used for immunoblots were as follows: anti-SOD1 (Stressgen, SOD-100, and Calbiochem, 574597), kinesin C2 (Affinity BioReagents) and CRMP-2 (Immuno-Biological Laboratories). Anti-ChAT (AB144P), KHC (MAB1614), KLC (MAB1617), synaptophysin (MAB5258-20UG), actin (MAB1501), Neurofilament-M (AB1987) and MBP (myelin basic protein, AB9046) antibodies were all purchased from Chemicon. Anti-KAP3, KIF3A, KIF3B, p150^{Glued}, p50 dynamitin, dynein IC, KIF2 and Rab3 antibodies were purchased from BD PharMingen/Transduction Laboratories. Primary antibodies used for immunoprecipitation and immunostaining were anti-SOD1 (Stressgen, SOD-100), ChAT (Chemicon, AB144P) and FLAG (Sigma, F3165) antibodies. KAP3 antibody was prepared by immunizing rabbits with a peptide containing the 1–14 amino acids of mouse KAP3, which are conserved in human KAP3, followed by affinity purification using an epitope-conjugated column.

Animals

We used the G1L line of transgenic mice harboring the G93A-mutated human *SOD1* gene (B6SJL-*TgN*(*SOD1-G93A*)1Gur^{dl}) purchased from the Jackson Laboratories. Mice harboring wild-type human *SOD1* gene (B6.Cg-*Tg*(*SOD1*)2Gur/J) was a gift from Dr Kawamata of Kyoto University. C57BL/6J mice were also used. The transgenic mice were backcrossed with C57BL/6J for more than 14 generations. All data were derived from male mice. All the animal experiments were approved by the Animal Care Committee of National Center of Neurology and Psychiatry (NCNP).

Preparation of subsegments from mouse spinal cords using LMD technique

Frozen sections from mouse spinal cords were prepared without fixation and processed through AS LMD (Leica) as previously described (17). Five sections were pooled for each sample location for subsequent analyses.

Isolation of misfolded SOD1 species from ventral white matter of spinal cords

The spinal cord was dissected from the indicated mice, and the ventral half of white matter at L1-S3 level was carefully dissected under a microscope. The dissected samples were homogenized in 300 μl of Nz homogenization buffer [20 mM HEPES, pH 7.4, 120 mM NaCl, 2 mM EDTA, pH 8.0, 0.25% NP-40 and complete protease inhibitor cocktail (Roche)] followed by a brief sonication., The lysates were added to 3.2 ml of Nycodenz linear density gradient in 10 mM HEPES, pH 7.4 and 1 mM EDTA, pH 8.0 (initial concentration of Nycodenz was 30%). After a centrifugation at 87 479*g* for 2 h at 4°C, in Optima MAX-E using MLS 50 rotor (Beckman Coulter), 160 μl of aliquot was collected from the top to the bottom of the tube, totaling 22 fractions. Twenty microliters of each fraction was collected and analyzed by immunoblot.

Immunoprecipitation

Affinity-purified anti-KAP3 and anti-SOD1 antibodies were captured with Dynabeads Protein G (Dynal Biotech) and cross-linked using dimethyl pimelimidate as per manufacturer's protocol. For the immunoprecipitation from fractions prepared from Nycodenz density gradient centrifugation, 30 μl of each fraction was mixed with the antibody-conjugated Dynabeads in 20 mM HEPES, pH 7.4, 120 mM NaCl, 2 mM EDTA and complete protease inhibitor cocktail. The mixture was incubated overnight at 4°C on a rocking platform, followed by washing with PBS containing 0.05% Tween-20. The target proteins were eluted with 30 μl of 0.1 M citric acid (pH 2.0) for 2 min, and half of the eluates

were analyzed. For the immunoprecipitation from spinal cords or SOD1-transfected PNG3 cells, tissues or cells were lysed in TN-T buffer (50 mM Tris–HCl, pH 7.6, 1% Triton X-100, 150 mM NaCl) containing complete protease inhibitor cocktail and subjected to a centrifugation at 5000*g* for 10 min at 4°C. The supernatants were incubated with antibody-conjugated Protein G Dynabeads and analyzed as described above.

Preparation of transported components from ventral cauda equina

The fraction enriched with transported components within motor axons was prepared from ventral roots of caudal spinal cords as described (41) with the following modifications. Ventral cauda equina was minced for two times in 400 μl of IM-D buffer supplemented with 1 mM ATP and a protease inhibitor cocktail (Complete; Roche) for 10 min on ice. They were subsequently subjected to centrifugation at 5000*g* for 10 min at 4°C. The obtained supernatants were measured for protein concentration and 5 μg of each was subjected to SDS/PAGE to evaluate the kinesin-2 contents. To analyze kinesin-2 status, the transported vesicle fractions prepared from four mice were subjected to 4.4 ml of sucrose step gradient centrifugation ranging from 0.2 to 2%. After centrifugation in an SW55 Ti rotor (Beckman Coulter) at 50 000 rpm for 18 h at 4°C, 400 μl of each fraction was collected from top of the tube, totaling 12 fractions, and 20 μl of each fraction was analyzed by SDS–PAGE/immunoblots.

Cell culture and transfection

NG108-15 cells (a kind gift from Dr Akazawa in Tokyo Medical and Dental University), a hybrid cell line of mouse N18TG2 neuroblastoma cells and rat C6-BU-1 glioma cells, were cultured in Dulbecco's modified Eagle's medium (DMEM) (Sigma, D5796) containing 10% fetal bovine serum and 2% HAT supplement (GIBCO). Differentiation of PNG3, a subclone of NG108-15 isolated from single cells, was induced with 1 mM of dibutyryl cAMP (Nacalai tesque) and 0.2 μM of dexamethasone (MB Biomedicals) for 3 days. Transfection of plasmids into PNG3 was performed using Optifect or Lipofectamine 2000 (Invitrogen Life Technologies) as per manufacturer's protocol. Culture medium was changed every 20–24 h except where indicated otherwise. Transfection of siRNA and co-transfection of siRNA with plasmids were performed according to the manufacturer's protocols using DharmaFECT transfection reagent 2 (Dharmacon) and DharmaEFCT Duo transfection reagent, respectively. For induction of SOD1 misfolding/aggregation, cells were treated with 6.5 μM of MG132 (a proteasome inhibitor) 56 h after transfection and then treated with 2.5 mM hydrogen peroxide for 2 h at 72 h after transfection. Cells were then lysed with TN-T buffer plus Complete protease inhibitor cocktail and subjected to centrifugation at 10 000*g* for 10 min at 4°C to be separated into soluble (supernatant) and insoluble (pellet) fractions.

Measurement of [^{3}H]ACh release

Depolarization-induced [^{3}H]ACh release was measured based on the method previously described (Kumagai *et al.*, 1993) with several modifications. For metabolic labeling of PNG3 cells by [^{3}H]choline, DMEM lacking choline chloride was used. Time schedules for labeling, reagents used and incubation time are shown in Figure 6C.

The culture medium was changed to choline-free DMEM either with or without colchicine. After 2 h incubation, 6.25 kBq [^{3}H]choline chloride ([methyl-^{3}H] choline chloride, 2.2 TBq/mmol; GE Healthcare) was added to the medium of each well of a 12-well plate. After 2 h incubation, the medium was changed to ACh release measuring buffer [20 mM HEPES-NaOH, pH 7.4, 150 mM NaCl, 5 mM KCl, 1.8 mM $CaCl_2$, 0.8 mM $MgSO_4$, 25 mM glucose, 25 μM eserine sulfate and 10 μM hemicholinium-3 (HC-3)] and the culture plates were returned to the CO_2 incubator. Eserine, an inhibitor for cholinesterase, was added to inhibit a degradation of released ACh by cholinesterase. HC-3, an inhibitor for high-affinity choline transporter 1, was added to completely inhibit [^{3}H]choline uptake after changing the medium. After 15 min incubation, with eserine and HC-3, an aliquot of culture medium was transferred into a 1.5 ml tube (media before KCl addition), and then KCl was added into the medium to a final concentration of 50 mM. The culture plates were quickly returned to the CO_2 incubator, and after 15 min, the medium was transferred into a new 1.5 ml tube (media after KCl addition). Both the medium collected before and after KCl addition were centrifuged at 10 000*g* for 5 min at 4°C to remove debris. The supernatants were mixed with a scintillation cocktail (Ultima Gold XR, Perkin Elmer) to measure the [^{3}H] radioactivity using a liquid scintillation spectrophotometer. The radioactivity of [^{3}H]ACh released by KCl was calculated by subtracting the activity of media before KCl (=S1) from the activity of media after KCl addition (=S2), as described in Figure 6C.

Immunocytochemistry

PNG3 cells were fixed with 4% paraformaldehyde in PBS for 15 min. After permeabilization with 0.15% Triton X-100 in PBS for 10 min, cells were treated with Blocking-one (Nacalai) for 1 h. The cells were then treated with primary antibodies in Blocking-one at 4°C overnight. The cells were washed with PBS. For detection, cells were treated with fluorescent-conjugated secondary antibodies in Blocking-one at room temperature for 1 h. After washing again with PBS, cells were mounted with Vectasheld (Vector Laboratories).

Autopsy specimens and immunohistochemistry

The studies were performed on archival, buffered 10% formalin-fixed, paraffin-embedded spinal cord tissues obtained at autopsy from four FALS patients who were members of two different families. Consent for autopsy was obtained from legal representatives in accordance with the requirements of local institutional review boards. The clinicopathological characteristics of the FALS patients have been previously reported (27,29). SOD1 gene analysis revealed that the members of the Japanese Oki family had a 2 bp deletion at codon 126 in the gene for SOD1 (frame-shift 126 mutation, D125X) and that the members of the T family had a Leucine to Valine substitution at codon 106 in the SOD1

gene (L106V). To look at the expression of KAP3 and SOD1 in these specimens, affinity-purified rabbit anti-KAP3 antibody (0.05 μg/ml, diluted 1:200 in 1% bovine serum albumin-containing PBS, pH 7.4), mouse monoclonal antibody against human SOD1 (0.5 mg/ml, clone1G_2, MBL, Aichi, Japan) and sheep polyclonal antibody against human SOD1 (1:20,000, Calbiochem, Darmstadt, Germany) were used as primary antibodies. Immunohistochemical reaction was performed by a standard procedure. Antibody signal was visualized by the avidin–biotin–immunoperoxidase complex (ABC) method using the appropriate Vectastain ABC Kit (Vector Laboratories, Burlingame, CA, USA) and 3,3′-diaminobenzidine tetrahydrochloride (DAB; Dako, Glostrup, Denmark) as the chromogen.

SUPPLEMENTARY MATERIAL

Supplementary Material is available at *HMG* online.

ACKNOWLEDGEMENTS

We wish to thank the laboratory members for helpful suggestions and Tomoko Dai, Mariko Soda, Yumiko Shimazaki and Tadatoshi Makino for their technical support.

Conflict of Interest statement. None declared.

FUNDING

This work was supported by research grants from RIKEN BSI, a Grant-in-Aid for Scientific Research on Priority Area (Advanced Brain Science Project) from the Ministry of Education, Culture, Sports, Science and Technology, NIBIO (Program for Promotion of Fundamental Studies in Health Sciences), a grant from Japan Foundation for Neuroscience and Mental Health and grants from the Ministry of Health, Labor and Welfare of Japan. Funding to pay the Open Access charge was provided by a grant from Ministry of Health, Labour and Welfare of Japan.

REFERENCES

1. Boillee, S., Vande Velde, C. and Cleveland, D.W. (2006) ALS: a disease of motor neurons and their nonneuronal neighbors. *Neuron*, **52**, 39–59.
2. Pasinelli, P. and Brown, R.H. (2006) Molecular biology of amyotrophic lateral sclerosis: insights from genetics. *Nat. Rev. Neurosci.*, **7**, 710–723.
3. Shaw, B.F. and Valentine, J.S. (2007) How do ALS-associated mutations in superoxide dismutase 1 promote aggregation of the protein? *Trends Biochem. Sci.*, **32**, 78–85.
4. Barber, S.C., Mead, R.J. and Shaw, P.J. (2006) Oxidative stress in ALS: a mechanism of neurodegeneration and a therapeutic target. *Biochim. Biophys. Acta.*, **1762**, 1051–1067.
5. Wang, J., Xu, G. and Borchelt, D.R. (2002) High molecular weight complexes of mutant superoxide dismutase 1: age-dependent and tissue-specific accumulation. *Neurobiol. Dis.*, **9**, 139–148.
6. Shibata, N., Asayama, K., Hirano, A. and Kobayashi, M. (1996) Immunohistochemical study on superoxide dismutases in spinal cords from autopsied patients with amyotrophic lateral sclerosis. *Dev. Neurosci.*, **18**, 492–498.
7. Watanabe, M., Dykes-Hoberg, M., Culotta, V.C., Price, D.L., Wong, P.C. and Rothstein, J.D. (2001) Histological evidence of protein aggregation in mutant SOD1 transgenic mice and in amyotrophic lateral sclerosis neural tissues. *Neurobiol. Dis.*, **8**, 933–941.
8. Jonsson, P.A., Graffmo, K.S., Andersen, P.M., Brannstrom, T., Lindberg, M., Oliveberg, M. and Marklund, S.L. (2006) Disulphide-reduced superoxide dismutase-1 in CNS of transgenic amyotrophic lateral sclerosis models. *Brain*, **129**, 451–464.
9. Koyama, S., Arawaka, S., Chang-Hong, R., Wada, M., Kawanami, T., Kurita, K., Kato, M., Nagai, M., Aoki, M., Itoyama, Y. *et al.* (2006) Alteration of familial ALS-linked mutant SOD1 solubility with disease progression: its modulation by the proteasome and Hsp70. *Biochem. Biophys. Res. Commun.*, **343**, 719–730.
10. Goldstein, L.S. and Yang, Z. (2000) Microtubule-based transport systems in neurons: the roles of kinesins and dyneins. *Annu. Rev. Neurosci.*, **23**, 39–71.
11. Hirokawa, N. and Takemura, R. (2005) Molecular motors and mechanisms of directional transport in neurons. *Nat. Rev. Neurosci.*, **6**, 201–214.
12. De Vos, K.J., Grierson, A.J., Ackerley, S. and Miller, C.C. (2008) Role of axonal transport in neurodegenerative diseases. *Annu. Rev. Neurosci.*, **31**, 151–173.
13. Collard, J.F., Cote, F. and Julien, J.P. (1995) Defective axonal transport in a transgenic mouse model of amyotrophic lateral sclerosis. *Nature*, **375**, 61–64.
14. Williamson, T.L. and Cleveland, D.W. (1999) Slowing of axonal transport is a very early event in the toxicity of ALS-linked SOD1 mutants to motor neurons. *Nat. Neurosci.*, **2**, 50–56.
15. Hafezparast, M., Klocke, R., Ruhrberg, C., Marquardt, A., Ahmad-Annuar, A., Bowen, S., Lalli, G., Witherden, A.S., Hummerich, H., Nicholson, S. *et al.* (2003) Mutations in dynein link motor neuron degeneration to defects in retrograde transport. *Science*, **300**, 808–812.
16. Puls, I., Jonnakuty, C., LaMonte, B.H., Holzbaur, E.L., Tokito, M., Mann, E., Floeter, M.K., Bidus, K., Drayna, D., Oh, S.J. *et al.* (2003) Mutant dynactin in motor neuron disease. *Nat. Genet.*, **33**, 455–456.
17. Tateno, M., Sadakata, H., Tanaka, M., Itohara, S., Shin, R.M., Miura, M., Masuda, M., Aosaki, T., Urushitani, M., Misawa, H. *et al.* (2004) Calcium-permeable AMPA receptors promote misfolding of mutant SOD1 protein and development of amyotrophic lateral sclerosis in a transgenic mouse model. *Hum. Mol. Genet.*, **13**, 2183–2196.
18. Baqri, R., Charan, R., Schimmelpfeng, K., Chavan, S. and Ray, K. (2006) Kinesin-2 differentially regulates the anterograde axonal transports of acetylcholinesterase and choline acetyltransferase in *Drosophila*. *J. Neurobiol.*, **66**, 378–392.
19. Ray, K., Perez, S.E., Yang, Z., Xu, J., Ritchings, B.W., Steller, H. and Goldstein, L.S. (1999) Kinesin-II is required for axonal transport of choline acetyltransferase in *Drosophila*. *J. Cell Biol.*, **147**, 507–518.
20. Hirokawa, N. (2000) Stirring up development with the heterotrimeric kinesin KIF3. *Traffic*, **1**, 29–34.
21. Blusztajn, J.K. and Wurtman, R.J. (1983) Choline and cholinergic neurons. *Science*, **221**, 614–620.
22. McGee, R., Simpson, P., Christian, C., Mata, M., Nelson, P. and Nirenberg, M. (1978) Regulation of acetylcholine release from neuroblastoma × glioma hybrid cells. *Proc. Natl Acad. Sci. USA*, **75**, 1314–1318.
23. Tojima, T., Yamane, Y., Takahashi, M. and Ito, E. (2000) Acquisition of neuronal proteins during differentiation of NG108-15 cells. *Neurosci. Res.*, **37**, 153–161.
24. Johnston, J.A., Dalton, M.J., Gurney, M.E. and Kopito, R.R. (2000) Formation of high molecular weight complexes of mutant Cu, Zn-superoxide dismutase in a mouse model for familial amyotrophic lateral sclerosis. *Proc. Natl Acad. Sci. USA*, **97**, 12571–12576.
25. Puttaparthi, K., Wojcik, C., Rajendran, B., DeMartino, G.N. and Elliott, J.L. (2003) Aggregate formation in the spinal cord of mutant SOD1 transgenic mice is reversible and mediated by proteasomes. *J. Neurochem.*, **87**, 851–860.
26. Haraguchi, K., Hayashi, T., Jimbo, T., Yamamoto, T. and Akiyama, T. (2006) Role of the kinesin-2 family protein, KIF3, during mitosis. *J. Biol. Chem.*, **281**, 4094–4099.
27. Kato, S., Shimoda, M., Watanabe, Y., Nakashima, K., Takahashi, K. and Ohama, E. (1996) Familial amyotrophic lateral sclerosis with a two base pair deletion in superoxide dismutase 1: gene multisystem degeneration with intracytoplasmic hyaline inclusions in astrocytes. *J. Neuropathol. Exp. Neurol.*, **55**, 1089–1101.
28. Kato, S., Hayashi, H., Nakashima, K., Nanba, E., Kato, M., Hirano, A., Nakano, I., Asayama, K. and Ohama, E. (1997) Pathological

characterization of astrocytic hyaline inclusions in familial amyotrophic lateral sclerosis. *Am. J. Pathol.*, **151**, 611–620.
29. Kato, S. (2008) Amyotrophic lateral sclerosis models and human neuropathology: similarities and differences. *Acta Neuropathol.*, **115**, 97–114.
30. Rich, M.M., Wang, X., Cope, T.C. and Pinter, M.J. (2002) Reduced neuromuscular quantal content with normal synaptic release time course and depression in canine motor neuron disease. *J. Neurophysiol.*, **88**, 3305–3314.
31. Brandon, E.P., Lin, W., D'Amour, K.A., Pizzo, D.P., Dominguez, B., Sugiura, Y., Thode, S., Ko, C.P., Thal, L.J., Gage, F.H. *et al.* (2003) Aberrant patterning of neuromuscular synapses in choline acetyltransferase-deficient mice. *J. Neurosci.*, **23**, 539–549.
32. Wang, J., Xu, G., Li, H., Gonzales, V., Fromholt, D., Karch, C., Copeland, N.G., Jenkins, N.A. and Borchelt, D.R. (2005) Somatodendritic accumulation of misfolded SOD1-L126Z in motor neurons mediates degeneration: alphaB-crystallin modulates aggregation. *Hum. Mol. Genet.*, **14**, 2335–2347.
33. Dupuis, L., de Tapia, M., Rene, F., Lutz-Bucher, B., Gordon, J.W., Mercken, L., Pradier, L. and Loeffler, J.P. (2000) Differential screening of mutated SOD1 transgenic mice reveals early up-regulation of a fast axonal transport component in spinal cord motor neurons. *Neurobiol. Dis.*, **7**, 274–285.
34. Teuchert, M., Fischer, D., Schwalenstoecker, B., Habisch, H.J., Bockers, T.M. and Ludolph, A.C. (2006) A dynein mutation attenuates motor neuron degeneration in SOD1(G93A) mice. *Exp. Neurol.*, **198**, 271–274.
35. Kieran, D., Hafezparast, M., Bohnert, S., Dick, J.R., Martin, J., Schiavo, G., Fisher, E.M. and Greensmith, L. (2005) A mutation in dynein rescues axonal transport defects and extends the life span of ALS mice. *J. Cell Biol.*, **169**, 561–567.
36. Deacon, S.W., Serpinskaya, A.S., Vaughan, P.S., Lopez Fanarraga, M., Vernos, I., Vaughan, K.T. and Gelfand, V.I. (2003) Dynactin is required for bidirectional organelle transport. *J. Cell Biol.*, **160**, 297–301.
37. Pantelidou, M., Zographos, S.E., Lederer, C.W., Kyriakides, T., Pfaffl, M.W. and Santama, N. (2007) Differential expression of molecular motors in the motor cortex of sporadic ALS. *Neurobiol. Dis.*, **26**, 577–589.
38. Maselli, R.A., Wollman, R.L., Leung, C., Distad, B., Palombi, S., Richman, D.P., Salazar-Grueso, E.F. and Roos, R.P. (1993) Neuromuscular transmission in amyotrophic lateral sclerosis. *Muscle Nerve*, **16**, 1193–1203.
39. Balice-Gordon, R.J., Smith, D.B., Goldman, J., Cork, L.C., Shirley, A., Cope, T.C. and Pinter, M.J. (2000) Functional motor unit failure precedes neuromuscular degeneration in canine motor neuron disease. *Ann. Neurol.*, **47**, 596–605.
40. Shimizu, K., Kawabe, H., Minami, S., Honda, T., Takaishi, K., Shirataki, H. and Takai, Y. (1996) SMAP, an Smg GDS-associating protein having arm repeats and phosphorylated by Src tyrosine kinase. *J. Biol. Chem.*, **271**, 27013–27017.
41. Takeda, S., Yamazaki, H., Seog, D.H., Kanai, Y., Terada, S. and Hirokawa, N. (2000) Kinesin superfamily protein 3 (KIF3) motor transports fodrin-associating vesicles important for neurite building. *J. Cell Biol.*, **148**, 1255–1265.
42. Jimbo, T., Kawasaki, Y., Koyama, R., Sato, R., Takada, S., Haraguchi, K. and Akiyama, T. (2002) Identification of a link between the tumour suppressor APC and the kinesin superfamily. *Nat. Cell Biol.*, **4**, 323–327.
43. Teng, J., Rai, T., Tanaka, Y., Takei, Y., Nakata, T., Hirasawa, M., Kulkarni, A.B. and Hirokawa, N. (2005) The KIF3 motor transports N-cadherin and organizes the developing neuroepithelium. *Nat. Cell Biol.*, **7**, 474–482.
44. Urushitani, M., Kurisu, J., Tsukita, K. and Takahashi, R. (2002) Proteasomal inhibition by misfolded mutant superoxide dismutase 1 induces selective motor neuron death in familial amyotrophic lateral sclerosis. *J. Neurochem.*, **83**, 1030–1042.
45. Kumagai-Tohda, C., Tohda, M. and Nomura, Y. (1993) Increase in neurite formation and acetylcholine release by transfection of growth-associated protein-43 cDNA into NG108-15 cells. *J. Neurochem.*, **61**, 526–532.

Neurochemistry International xxx (2010) xxx–xxx

Contents lists available at ScienceDirect

Neurochemistry International

journal homepage: www.elsevier.com/locate/neuint

Familiar amyotrophic lateral sclerosis (FALS)-linked SOD1 mutation accelerates neuronal cell death by activating cleavage of caspase-4 under ER stress in an *in vitro* model of FALS

Yoshihisa Koyama [a,1], Toru Hiratsuka [a,1], Shinsuke Matsuzaki [a,b,1], Satoru Yamagishi [a], Shinsuke Kato [c], Taiichi Katayama [b,*], Masaya Tohyama [a,b]

[a] Department of Anatomy and Neuroscience, Graduate School of Medicine, Osaka University, 2-2 Yamadaoka, Suita, Osaka 565-0871, Japan
[b] Department of Child Development and Molecular Brain Science, United Graduate School of Child Development, Osaka University, Kanazawa University and Hamamatsu University School of Medicine, 2-2 Yamadaoka, Suita, Osaka 565-0871, Japan
[c] Department of Neuropathology, Institute of Neurological Sciences, Faculty of Medicine, Tottori University, Yonago, Tottori 683-8503, Japan

ARTICLE INFO

Article history:
Received 24 June 2010
Received in revised form 22 August 2010
Accepted 27 August 2010
Available online xxx

Key words:
ALS
ER stress
Human
Neuronal cell death
Caspase-4

ABSTRACT

Recently, endoplasmic reticulum (ER) dysfunction has been implicated in the pathogenesis of familial amyotrophic lateral sclerosis (FALS). Although up-regulation of caspase-12 has been reported in G93A SOD1 transgenic mice, it is controversial whether similar mechanisms operate in human FALS. We found that ER stress in cells stably expressing L84V SOD1 induces neuronal cell death and accelerates cleavage of caspase-4. We also detected oligomer formation of L84V SOD1 in L84V SOD1-expressing human neuroblastoma cells. These findings show that ER stress in L84V SOD1-expressing human cells causes the aggregation and inclusion bodies of L84V SOD1 to induce neuronal death through the accelerated cleavage of caspase-4.

1. Introduction

Amyotrophic lateral sclerosis (ALS) is a neurodegenerative disorder, clinically characterized by progressive dysfunction of either upper or lower limb, beginning in middle age. Pathologically, severe motor neuronal loss is found in the ALS spinal cord. About 10% of cases of ALS are inherited, usually as autosomal dominant trait, a disorder known as familiar ALS (FALS) (Gurney, 2000; Brown and Robberecht, 2001; Cleveland and Rothstein, 2001; Rowland and Schneider, 2001; Bruijin et al., 2004). More than 20% of FALS cases are associated with mutation of the Cu/Zn-superoxide dismutase (SOD) (Rosen et al., 1993). Nearly 100 different mutations in the SOD1 gene have been identified in FALS patients. Neuronal Lewy body-like hyaline inclusions (LBHI) containing mutant SOD1 are morphological hallmarks of FALS associated with mutant SOD1, although little is known about the formation of LBHI in neurons (Bruijin et al., 2004). We recently reported that ER stress induces the appearance of LBHI-like inclusions (LBHI-I) in human neuroblastoma (SK-N-SH) cells expressing SOD1 with the L84V (L84V SOD1) mutation associated with FALS (Yamagishi et al., 2007). These LBHI-I closely resemble LBHI in patients with SOD1-linked FALS, because LBHI-I and LBHI share the similar cytological and immunohistochemical characteristics (Yamagishi et al., 2007). Furthermore, there is evidence demonstrating that ER stress plays an important role in the pathogenesis of FALS. Up-regulation of Bip in the spinal motor neurons of H46R (H46R SOD1) and L84V SOD1 transgenic mice (Tobisawa et al., 2003; Atkin et al., 2006), and up-regulation of the ER-resident protein disulfide isomerase (PDI) family members in the lumbar spinal cords of G93A SOD1 transgenic mice (Wate et al., 2005) have been reported. Moreover, Ilieva et al. reported that oxydative and ER stress interplay in sporadic ALS (Ilieva et al., 2007). Based upon these findings, it is likely that the LBHI seen in human patients with mutant SOD1-linked FALS arise from ER dysfunction.

On the other hand, we have shown that familial AD (FAD)-linked PS1 mutations increase vulnerability to ER by altering the unfolded-protein response (UPR) (Katayama et al., 1999; Sato et al., 2001). Although caspase-12 has been shown to be involved in signaling pathways specific to ER stress-induced apoptosis in rodents (Nakagawa et al., 2000), caspase-12 protein is not produced in humans (Fischer et al., 2002). Accordingly, caspase-12 does not function in ER stress-induced apoptosis associated with FAD. Recently, we revealed that FAD-linked PS1 mutation accelerates the cleavage of caspase-4 under ER stress to induce

* Corresponding author. Tel.: +81 6 6879 3313.
E-mail address: katayama@ugscd.osaka-u.ac.jp (T. Katayama).
[1] Contributed equally to this work.

0197-0186/$ – see front matter © 2010 Elsevier Ltd. All rights reserved.
doi:10.1016/j.neuint.2010.08.023

Please cite this article in press as: Koyama, Y., et al., Familiar amyotrophic lateral sclerosis (FALS)-linked SOD1 mutation accelerates neuronal cell death by activating cleavage of caspase-4 under ER stress in an *in vitro* model of FALS. Neurochem. Int. (2010), doi:10.1016/j.neuint.2010.08.023

neuronal cell death (Hitomi et al., 2004; Yukioka et al., 2008). However, it is still unclear whether ER stress causes neuronal death in FALS. Although up-regulation of caspase-12 in G93A SOD1 mice has been reported (Wootz et al., 2004), direct evidence indicating that ER stress causes neuronal death, and that, as has been demonstrated in FAD, caspase-4 can function as an ER stress-induced caspase and is involved in the pathogenesis of FALS, is lacking. In the present study, using an *in vitro* model for FALS (L84V-expressing human neuroblastoma cells), we found that the L84V SOD1 mutation accelerates cleavage of caspase-4 to induce neuronal death under conditions of ER stress, that ER stress in L84V SOD1-expressing cells causes oligomer formation by L84V SOD1, and that ER stress in these cells increases the number of LBHI-I exhibiting SOD1 and ubiquitin immunoreactivity. This suggests that ER stress in L84V SOD1-expressing human cells causes the aggregation of L84V SOD1 in the inclusion bodies to induce neuronal death.

2. Results

2.1. L84V SOD1 mutation increases vulnerability to ER stress

Before examining the effect of L84V SOD1 mutation on ER stress-induced cell death, we generated SK-N-SH human neuroblastoma cell lines that stably express FLAG-tagged human L84V SOD1 mutation associated with FALS (Aoki et al., 1995). Western blot analysis confirmed that expression of endogenous and exogenous SOD1 was equal in the cell line (Yamagishi et al., 2007). We then added tunicamycin (TM), which induces ER stress by preventing protein glycosylation, to the medium. After the TM treatment, cell death increased in cells expressing L84V SOD1 compared with cells expressing the wild-type protein (Fig. 1A). On the other hand, the increase in cell death induced by hydrogen peroxide (data not shown) or staurosporine was not affected by expression of L84V SOD1 (Fig. 1B). These findings showed that the L84V SOD1 mutation increases vulnerability to ER stress.

Next we examined the effect of L84V SOD1 on ER stress-induced apoptosis at the morphological level 9.5 h after TM stimulation (Fig. 1C–H). Assessment of cell death was performed using a terminal deoxynucleotidyl transferase (TdT) dUTP nick-end labeling (TUNEL) method with an ApoTag *in situ* apoptosis detection kit (Oncor). As a result, TUNEL-positive cells were detected in both wild-type and L84V SOD1 cells 9.5 h after TM treatment (Fig. 1C), and the ratio of TUNEL-positive cells to total cells was significantly increased in L84V SOD1-expressing cells (to over 33%) more than in cells expressing wild-type SOD1 (Fig. 1D) 9.5 h after TM treatment. Moreover, to confirm that L84V SOD1 cells also undergo apoptosis morphologically, identification of apoptotic L84V SOD1 cells by hematoxylin–eosin (HE) staining was performed (Fig. 1E). Fig. 1E shows a representative apoptotic cell expressing L84V SOD1 with eosinophilic staining (Fig. 1E, arrow). Subsequent ultrastructural analysis of an apoptotic L84V SOD1 cell identified by HE staining, by electron microscopy, also showed that these cells exhibited typical apoptotic morphological changes, including nuclear fragmentation, chromatin condensation (Fig. 1F and H, arrows), the appearance of many vacuoles (Fig. 1F, arrow heads) and cell shrinkage. Surprisingly, electron microscopic analysis revealed ER located at the periphery of the cytoplasm of apoptotic cells, namely eosinophilic apoptotic bodies (Fig. 1F and G, arrows).

Thus, these results revealed that the L84V SOD1 mutation specifically increases vulnerability to ER stress and cell death by apoptosis.

2.2. L84V SOD1 mutation accelerates the cleavage of caspase-4 under ER stress

To examine whether caspase-4 was specifically cleaved from L84V SOD1-expressing cells under ER stress, we compared the cleavage of caspase-4 between L84V SOD1 and wild-type SOD1-expressing cells under TM treatment, and we also compared the cleavage of caspase-4 in cells expressing L84V SOD1 with and without TM treatment. In the wild-type SOD1 cells, final cleavage products of procaspase-4 (Fig. 2A, left panel arrow) could not be detected under the basal condition, and increased gradually after the addition of TM (Fig. 2A, left panel). In the cells expressing L84V SOD1, the cleaved form of caspase-4 was detected in the basal condition (Fig. 2A, right). L84V SOD1 expression increased the cleavage of procaspase-4 time-dependently under TM treatment, compared with that found in cells expressing wild-type SOD1 (Fig. 2A, right). In contrast, when cells expressing L84V SOD1 were exposed to non-ER stress, staurosporine at a dose providing a similar extent of cell death to that induced by TM, final cleavage products of procaspase-4 were not observed (Fig. 2B). Densitometric analyses of cleaved-caspase-4 revealed a significant difference between wild-type SOD1-expressing cells and L84V SOD1-expressing cells at 3 and 6 h after TM treatment (Fig. 2C).

2.3. ER stress accelerates the aggregation of L84V SOD1 under ER stress

To determine the state of aggregated mutant SOD1 in the inclusion body, we applied native-polyacrylamide gel electrophoresis (native-PAGE) to L84V and wild-type SOD1-expressing SK-N-SH cells treated with TM.

Comparing the position of wild-type SOD1 after TM treatment on the gel with those of protein makers, a single thick band at an apparent molecular weight of about 15 kDa, corresponding to the molecular weight of SOD1, was found, but no oligomer formation by denatured wild-type SOD1 was detected (Fig. 2D, $SOD1^{WT}$). On the other hand, when L84V SOD1 was examined, oligomers of L84V SOD1 were observed (Fig. 2D, $SOD1^{L84V}$). Judging from the molecular weights and specificity of SOD-positive bands by Western blot analysis, these bands likely represent dimers, trimers and higher molecular weight oligomers of L84V SOD1 (Fig. 2D, $SOD1^{L84V}$).

3. Discussion

3.1. L84V SOD1 mutation increases vulnerability to ER stress

If LBHI-I is associated with the pathogenesis of ALS, cells with LBHI-I would be vulnerable like the motor neurons in the spinal cords of ALS patients and SOD1 mutant transgenic mice. However, it has been unclear whether our human neuroblastoma cells expressing L84V SOD1, which have LBHI-I, are more vulnerable to ER stress than wild-type SOD1-expressing cells. We performed a cell death assay using cells expressing L84V SOD1 and wild-type SOD1. Cell death increased in cells expressing L84V SOD1 compared with cells expressing the wild-type protein. ER stress is suspected to be involved in the neuronal death occurring in various neurodegenerative diseases, such as Alzheimer's disease (AD) (Katayama et al., 1999; Sato et al., 2001), ischemia (Bando et al., 2003), Huntington's disease (Kouroku et al., 2002), ALS (Kanekura et al., 2009) and Parkinson's disease (Ryu et al., 2002). Regarding the pathogenesis of FALS, neuronal LBHI seen in a human patient with L84V SOD1-linked FALS were shown to be caused by ER dysfunction in human neuroblastoma cells and L84V SOD1 transgenic mice (Yamagishi et al., 2007), and significant up-regulation of the ER-resident protein disulfide isomerase (PDI)

Please cite this article in press as: Koyama, Y., et al., Familiar amyotrophic lateral sclerosis (FALS)-linked SOD1 mutation accelerates neuronal cell death by activating cleavage of caspase-4 under ER stress in an *in vitro* model of FALS. Neurochem. Int. (2010). doi:10.1016/j.neuint.2010.08.023

family members was shown in the lumbar spinal cord of transgenic G93A SOD1 model mice for FALS (Atkin et al., 2006). In this experiment, aggregates of SOD1 and formation of LBHI-I were shown in L84V SOD1-expressing cells, induced by ER stress, as we had shown in a previous study. Prolonged ER stress subsequently activated the apoptotic pathway, resulting in cell death. We analyzed activation of caspase-4 in these cells. As expected, the SOD aggregates of L84V SOD1-expressing cells colocalized with caspase-4. Indeed, apoptotic morphological changes were observed in cells with SOD aggregates; however, we detected no activation of caspase-4 in cells with LBHI-I (data not shown). Therefore, caspase-4 is associated with aggregation, but inclusions are not directly related to caspase-4 activation. At any rate, the present study showed that the L84V SOD1 mutation expressed in FALS increases neuronal vulnerability to ER stress. Thus, the ER may be important for regulating intracellular apoptotic signaling in neurons of FALS patients, as has been revealed in AD, ischemia, Parkinson's disease and Huntington's disease.

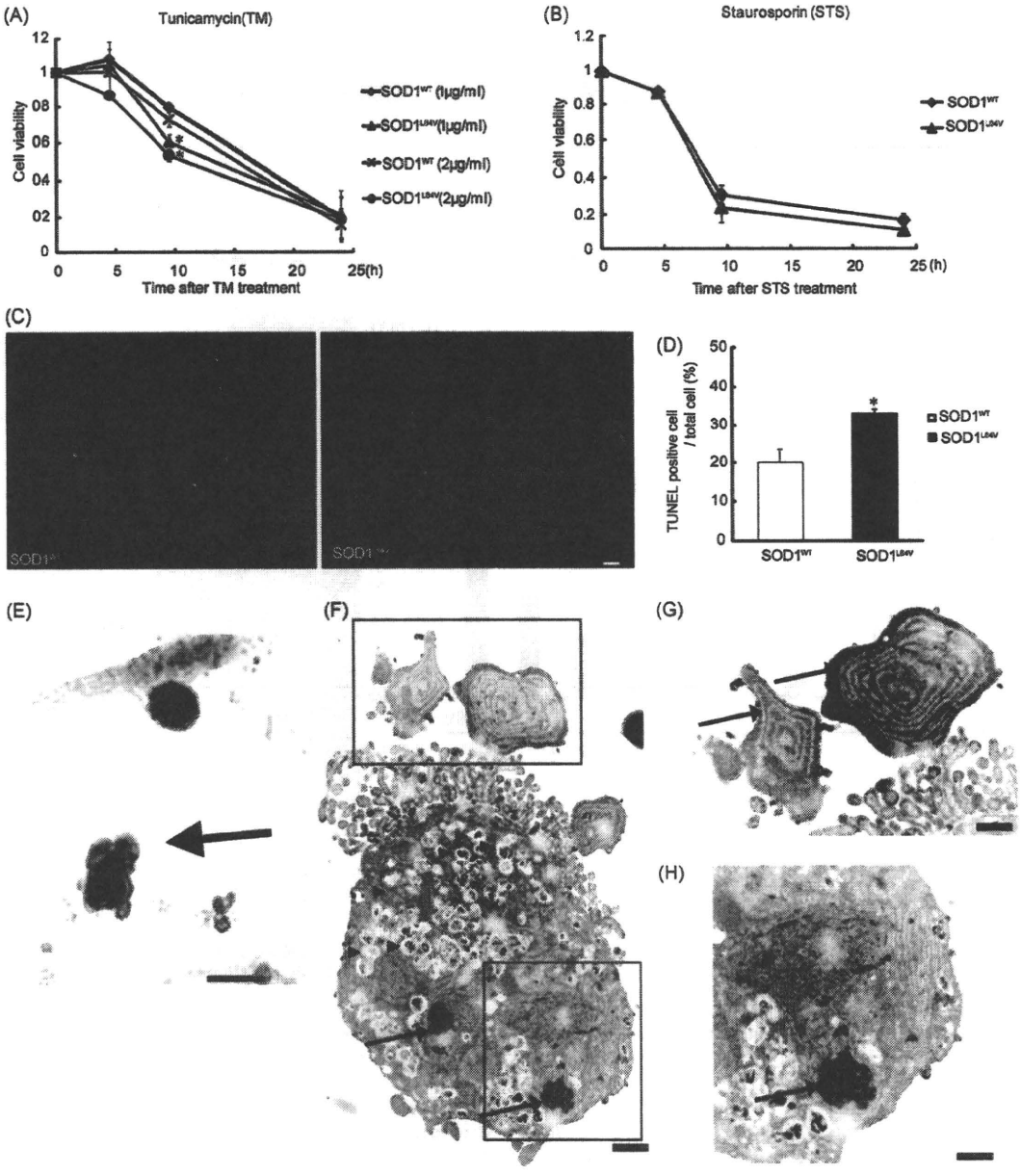

Fig. 1. L84V SOD1 mutation alters sensitivity to ER stress. Cell viability of both wild-type and L84V SOD1-expressing cells for the indicated period after 1 or 2 μg/ml tunicamycin (TM) treatment using the WST-1 activity assay (A), or after 0.5 μM staurosporine treatment using an assay based on the morphological change (B). These data represent the means ± S.E.M. of five independent experiments. Asterisks show a significant difference from wild-type SOD1 ($SOD1^{WT}$). Asterisks indicate $P < 0.01$ by the Student's *t*-test. (C) The L84V SOD1 mutation expression accelerates apoptosis 9.5 h after TM treatment. Significantly more TUNEL-positive nuclei are observed in L84V SOD1-expressing cells (left panel) than in wild-type SOD1-expressing cells (right panel) under TM treatment. Scale bar = 50 μm. (D) The extent of cell death assessed by TUNEL staining, and expressed as the means ± S.E.M. of three independent experiments. Asterisks show a significant difference from wild-type SOD1. Asterisks indicate $P < 0.01$. (E) Identification of the apoptotic L84V SOD1-expressing cells (arrow) under TM stimulation using hematoxylin–eosin (HE) staining at the light microscopic level. Scale bar = 100 μm. (F) Electron microscopy showing the apoptotic L84V SOD1-expressing cells after TM treatment. A number of vacuoles (arrow head), chromatin condensation and nuclear fragmentation (arrow) are seen. Eosinophilic apoptotic bodies contained ER, which shows an aberrant distribution (G; enlargement of the upper square in (F), arrow) and chromatin condensation (H; enlargement of the lower square in (F), arrow) at the higher magnification. Scale bar = 10 μm (F) and 5 μm (G and H).

Please cite this article in press as: Koyama, Y., et al., Familiar amyotrophic lateral sclerosis (FALS)-linked SOD1 mutation accelerates neuronal cell death by activating cleavage of caspase-4 under ER stress in an *in vitro* model of FALS. Neurochem. Int. (2010), doi:10.1016/j.neuint.2010.08.023

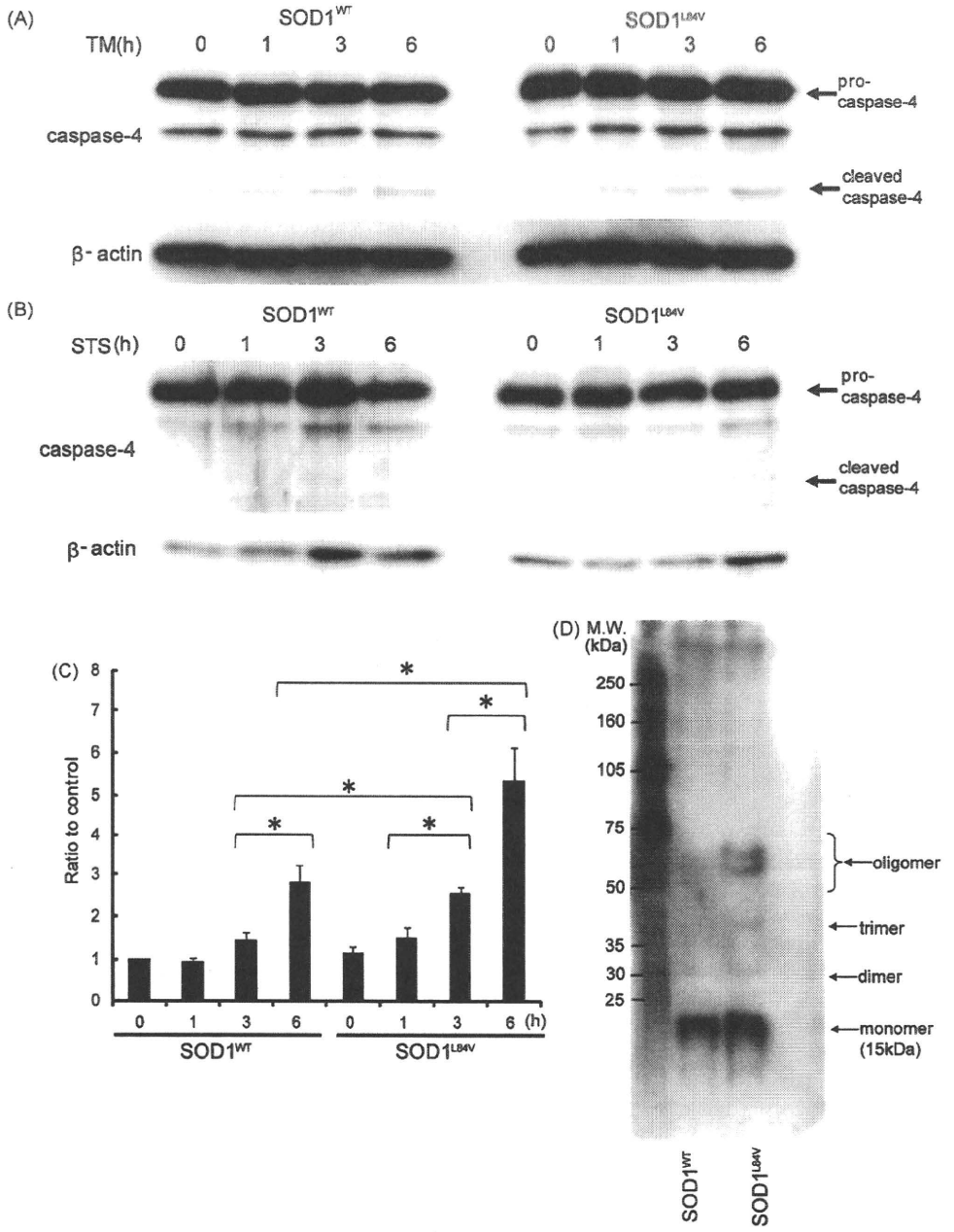

Fig. 2. L84V SOD1 accelerates the cleavage of caspase-4 under ER stress. SK-N-SH cells stably expressing wild-type SOD1 ($SOD1^{WT}$) (A, left panel) and L84V SOD1 mutation ($SOD1^{L84V}$) (A, right panel) were treated with 1 μg/ml tunicamycin (TM) followed by incubation for the indicated periods. (B) Non-ER stress. Staurosporine does not induce an increase in the cleavage of caspase-4. Equal amounts of cell lysates were analyzed by Western blotting using anti-caspase-4 and β-actin antibody. (C) Densitometric analyses of Western blot results (A). *$P < 0.01$ for comparison with wild-type SOD1 cells, by the Student's *t*-test. (D) Oligomer formation by SOD1 protein in both wild-type and L84V SOD1-expressing cells at 21 h after 1 μg/ml TM treatment using native-PAGE. M.W., molecular weight marker. The volume of loaded markers was 5 μl. The quantity of protein was 15–25 μg.

3.2. L84V SOD1 mutation accelerates the cleavage of caspase-4 under ER stress

In rodents, caspase-12 mediates apoptosis specifically in response to ER stress (Nakagawa et al., 2000). A significant up-regulation of caspase-12 was also observed in transgenic G93A SOD1 ALS model mice (Atkin et al., 2006). However, caspase-12 protein is not produced in humans, because the gene is interrupted by a frame shift and premature stop codon; there is also an amino acid substitution in the critical site for caspase activity in humans (Fischer et al., 2002). Therefore, some other caspases with similar structure might substitute functionally for caspase-12 in humans. We have found that caspase-4 can function as an ER stress-induced caspase in humans (Hitomi et al., 2004). Subsequently, we have revealed that caspase-4 is involved in pathogenesis of AD, because a familial AD-linked mutation enhances the cleavage of caspase-4 (Yukioka et al., 2008). The present study demonstrated that a FALS-linked mutation (L84V SOD1 mutation) enhances the cleavage of caspase-4, suggesting that caspase-4 might play a key role in the pathogenesis of FALS.

Thus, caspase-4 is a key caspase for neuronal death in both AD and FALS, suggesting that cleavage of procaspase-4 may induce the

Please cite this article in press as: Koyama, Y., et al., Familiar amyotrophic lateral sclerosis (FALS)-linked SOD1 mutation accelerates neuronal cell death by activating cleavage of caspase-4 under ER stress in an *in vitro* model of FALS. Neurochem. Int. (2010), doi:10.1016/j.neuint.2010.08.023

neuronal cell death in ischemia, Parkinson's disease and Huntington's disease, because dysfunction of the ER causes the neuronal death in these diseases.

3.3. ER stress accelerates the aggregation of L84V SOD1 under ER stress

While the importance of ER stress or proteasome malfunction in the formation of mutant SOD1 aggregation has been suggested (Kato et al., 2000; Johnston et al., 2000; Julien, 2001; Hyun et al., 2003; Tobisawa et al., 2003; Kikuchi et al., 2006), the mechanism by which mutant SOD1 forms LBHI in FALS remains unclear. In this study using SK-N-SH cells, it is shown that mutant SOD1, but not the wild-type SOD1, forms oligomers under ER stress conditions. Thus, it is likely that ER stress to SK-N-SH cells expressing L84V SOD1 results in the formation of SOD1- and ubiquitin-immunoreactive inclusion bodies, which contain ER and oligomerized mutant SOD1. Because inclusion bodies with a similar character were observed in the motor neurons of L84V SOD1 transgenic mice, ER stress to neurons expressing mutant SOD1 produces LBHI composed of ER and oligomerized mutant SOD1, which induces the cell death. However, it remains unclear why the same type of stress induces different outcomes for mutant SOD1 aggregation in neuroblastoma cells. Alternatively, there are various reports about the relation between pathogenesis of ALS and the inclusion body of ALS so far. For example, it is known that protein TDP-43 is a component of ubiquitin-positive, tau-negative inclusions, that is different from SOD-positive inclusions (Arai et al., 2006; Mackenzie et al., 2007). Moreover, it was reported that organelle-derived inclusion bodies are associated with neurodegenerative diseases (Okado-Matsumoto and Fridovich, 2001; Sturtz et al., 2001; Nishimura et al., 2004; Kanekura et al., 2006; Filimonenko et al., 2007). Thus, to address above issue, we should obtain much more evidence related to ER function and the formation of aggregates. To date, we have found common features between the small aggregates in L84V SOD1-expressing SK-N-SH cells and neuronal LBHI-precursor in L84V transgenic mice, including regions of abnormal ER aggregation surrounded by abundant free ribosomes. Furthermore, in accordance with the findings of our previous study (Yamagishi et al., 2007), exposure to TM resulted in the development of a number of eosinophilic aggregates and inclusion bodies at the periphery of the cytoplasm of L84V SOD1-expressing SK-N-SH human neuroblastoma cells, but not in cells expressing wild-type SOD1. The aggregates and inclusion bodies were positive also for SOD1, ubiquitin, an ER retention signal (KEDL) protein and Bip (data not shown, see Yamagishi et al., 2007), showing that L84V SOD1 is localized in the aggregates, inclusion bodies and ER. Subsequent electron microscopic analysis revealed that eosinophilic aggregates and the inclusion bodies located at the periphery of the cytoplasm contained ER (data not shown) as described in our previous study (Yamagishi et al., 2007).

Thus, the results revealed that the L84V SOD1 mutation increases vulnerability to ER stress and the appearance of aggregates and inclusion bodies containing L84V SOD1 and ER. In conclusion, our *in vitro* model might shed light on the development of therapies that can prevent the progression of mutant SOD1-linked FALS.

4. Experimental procedures

4.1. Cell culture

Non-differentiated SK-N-SH human neuroblastoma cells were obtained from the Riken Cell Bank (Tsukuba, Japan), and were cultured in α-MEM (Invitrogen) containing 10% fetal bovine serum at 37 °C under 5% CO_2. These cells were transfected with pcDNA3.1-hSOD1 and pcDNA3.1-hL84V-SOD1 to cause overexpression of wild-type or L84V mutant SOD1, respectively. G418-resistant stable neuroblastoma cell lines expressing equal levels of endogenous and exogenous SOD1 were established. In all experiments, we used cultures that were at 70–80% confluence to avoid the influence of stress induced by overgrowth. On the day of stimulation, fresh medium was added more than 1 h before exposure to stress to ensure the same conditions for each culture.

4.2. Cell viability assay

4.2.1. WST-1 activity assay

L84V SOD1-expressing or WT cells (3×10^3) were plated onto a 96-well plate 36 h before the cell viability assay. Cells were treated with 1 or 2 μg/ml TM for the indicated periods shown in Fig. 1A, and 10 μl of WST-1 (Roche, Basel, Switzerland) was added to the medium and cultured for 3 h. Signal for WST-1 was determined by the absorption at a wavelength of 450–650 nm. Data are expressed as the means ± standard errors of the means (S.E.M.) for at least three independent experiments.

4.2.2. Assay based on the morphological change

Cell toxicity to WT cells and L84V cells treated with 40 and 80 μM H_2O_2 or 0.5 μM staurosporine for the indicated periods shown in Fig. 1B was assessed as follows. Cell death was evaluated on the basis of morphological changes observed by phase contrast microscopy or nuclear changes fluoroscopically detected after costaining the cells with 10 μM Hoechst 33342 and 10 μM propidium iodide (PI). Nuclear fragmentation was detected by Hoechst-positive staining and nuclear collapse was detected by PI-positive staining. Dead cells were identified on the basis of being double-positive. The staining was measured independently in three fields and at least 300 cells were counted. Data are expressed as the means ± S.E.M. for at least three independent experiments.

4.3. In situ detection of apoptosis

In situ detection of apoptotic cells was performed using a TUNEL method with a TMR red *in situ* cell death detection kit (Roche). Briefly, cells were washed in 0.1 M phosphate-buffered saline (PBS), fixed at room temperature (RT) for 1 h in 0.1 M PBS containing 4% paraformaldehyde (PFA), blocked with 0.1% sodium citrate buffer containing 0.1% Triton X for 2 min on ice, and incubated at 37 °C for 1 h with 50 μl of TUNEL reaction buffer from the Roche kit. The apoptotic cells were labeled with red fluorescent dye and counted using a fluorescence microscope. TUNEL-positive cells were expressed as a percentage of total cells. For each experiment, a minimum of five fields was examined.

4.4. Immunohistochemistry

Non-differentiated SK-N-SH cells stably expressing wild-type SOD1 or L84V SOD1 were treated with 1 or 2 μg/ml of TM for 24 h. Then, the cells were fixed with Zamboni's solution, rinsed in 0.1 M PBS, and incubated for 30 min in 0.3% H_2O_2 to eliminate endogenous peroxidases. Next, the cells were incubated overnight at 4 °C with an anti-SOD1 antibody (1:1000 dilution) (Chemicon, Temecula, CA), anti-KDEL antibody (1:500 dilution) (Stressgen, Victoria, BC, Canada) or anti-ubiquitin antibody (1:500 dilution) (Stressgen, Victoria, BC, Canada) in 0.1 M PBS containing 0.3% Triton X-100 and 3% bovine serum albumin (BSA). After washing in 0.1 M PBS, cells for detection of SOD1 were incubated for 30 min with biotinylated anti-sheep IgG (Vector Laboratories, Burlingame, CA). Following amplification with avidin–biotin complex from the ABC kit (Vector Laboratories), reaction products were visualized with 0.05 M Tris–HCl buffer containing 0.02% diaminobenzidine (DAB) and 0.1% hydrogen peroxide. Cells positive for KDEL or ubiquitin were incubated with fluorescent dye (Alexa Fluor 568)-conjugated goat anti-mouse IgG (for KDEL, 1:1000 dilution) or goat anti-rabbit IgG (for ubiquitin, 1:1000 dilution) (Molecular Probes, Eugene, OR) for 1 h at room temperature in 0.02 M PBS containing 3% BSA. Finally, the cells were counterstained with hematoxylin and eosin.

4.5. Electron microscopy

Wild-type or L84V SOD1-expressing cells were exposed to 1 μg/ml TM for 24 h and then fixed at RT for 1 h in 0.1 M phosphate buffer (PB) containing 2.5% glutaraldehyde and 2% PFA. After apoptotic L84V SOD1-expressing cells were identified by Mayer's hematoxylin and eosin (HE) staining, they were decolorized, rehydrated and rinsed in 0.1 M PB. Thereafter, the cells were post-fixed in 1% OsO_4 at RT for 1 h, dehydrated in a graded ethanol series, and embedded in epon resin (Quetol 812; Nisshin EM Co.). Areas containing apoptotic cells were block-mounted in epoxy-resin by the direct epoxy-resin embedding method (Yamagishi et al., 2007) and cut into 80-nm sections. The sections were counterstained with uranyl acetate and lead citrate and then examined using an H-7100 electron microscope (Hitachi).

4.6. Western blot analysis

Wild-type or L84V SOD1-expressing cells were harvested at 0, 1, 3 and 6 h after addition of 1 μg/ml TM, 40 and 80 μM H_2O_2 or 0.5 μM staurosporine, and then lysed in TNE buffer (50 mM Tris–HCl (pH 7.5), 1 mM EDTA (pH 8.0), 150 mM NaCl) containing 0.5% NP40. Protein samples (20 μg) were subjected to 12% SDS-PAGE and transferred to polyvinylidene difluoride filters (Millipore, Bedford, MA). The membranes were blocked with 0.1 M PBS containing 5% skim milk and 0.05%

Please cite this article in press as: Koyama, Y., et al., Familiar amyotrophic lateral sclerosis (FALS)-linked SOD1 mutation accelerates neuronal cell death by activating cleavage of caspase-4 under ER stress in an *in vitro* model of FALS. Neurochem. Int. (2010), doi:10.1016/j.neuint.2010.08.023

Tween20 for 1 h at RT and incubated overnight at 4 °C with a mouse monoclonal anti-caspase-4 primary antibody (1:1000; MBL, Raleigh, NC). After washing in 0.1 M PBS containing 0.05% Tween20, the membranes were then incubated for 1 h at RT with a HRP conjugated anti-mouse IgG secondary antibody (1:2000; Cell Signaling, Beverly, MA), visualized in ECL solution (GE Healthcare Bio-Sciences Corporation, Piscataway, NJ, USA) for 1 min, and exposed onto X-Omat film (FUJI, Kanagawa, Japan) for 1–3 min. Finally, the membranes were incubated in a stripping buffer (2% SDS, 0.7% β-mercaptoethanol, 62.5 mM Tris–HCl, pH 6.8) for 30 min at 65 °C and re-probed with a monoclonal mouse anti-β-actin (1:3000; Chemicon, Rosmont, IL) primary antibody and a HRP conjugated anti-mouse IgG secondary antibody as loading controls. Our Western blot bands showed the same band sizes as indicated in the antibody information sheets. Each protein level was quantified by densitometry (Image J, National Institutes of Health, USA) and normalized to the β-actin levels.

4.7. Native-polyacrylamide gel electrophoresis

Native-PAGE was performed as reported previously (Schagger, 2006; Wittig et al., 2006). Membrane protein (30–100 μg protein per gel lane) was resuspended in 0.2–0.5% n-dodecyl β-D-maltoside (DDM) (or alternate treatment as indicated) in buffer composed of 50 mM NaCl, 5 mM 6-aminohexanoic acid and 50 mM imidazole pH 7.0 and then clarified after 15 min at room temperature by microcentrifuge centrifugation for 5 min before addition of 0.5% Coomassie G250 (Sigma) and 50 mM 6-aminohexanoic acid. Samples were resolved on 4–16.5% gradient acrylamide gels with cooling; the anode buffer contained 25 mM imidazole pH 7.0 and the cathode buffer contained 50 mM tricine, 7.5 mM imidazole pH 7.0 with 0.02% Coomassie G250. High molecular mass standards for native electrophoresis were obtained from Amersham and were stained with Coomassie R250. Wild-type SOD1 and L84V SOD1 after 1 μg/ml of TM stimulation for 24 h were loaded onto a gel. Following electrophoretic transfer to a PVDF membrane (Immobilon-P, Millipore), proteins were identified by immunoblotting and detection with ECL as described above (see Section 4.6).

Acknowledgment

This work was supported by a Grant-in-Aid from the Ministry of Education, Culture, Sports, Science and Technology, Japan.

References

Arai, T., Hasegawa, M., Akiyama, H., Ikeda, K., Nonaka, T., Mori, H., Mann, D., Tsuchiya, K., Yoshida, M., Hashizume, Y., Oda, T., 2006. TDP-43 is a component of ubiquitin-positive tau-negative inclusions in frontotemporal lobar degeneration and amyotrophic lateral sclerosis. Biochem. Biophys. Res. Commun. 351, 602–611.

Atkin, J.D., Farg, M.D., Turner, B.J., Tomas, D., Lysaght, J.A., Nunan, J., Rembach, A., Nagley, P., Beart, P., Cheema, S.S., Horne, M.K., 2006. Induction of the unfolded protein response in familial amyotrophic lateral sclerosis and association of protein-disulfide isomerase with superoxide dismutase 1. J. Biol. Chem. 281, 30152–30165.

Aoki, M., Abe, K., Houi, K., Ogasawara, M., Matsubara, Y., et al., 1995. Variance of age at onset in a Japanese family with amyotrophic lateral sclerosis associated with a novel Cu/Zn superoxide dismutase mutation. Ann. Neurol. 37, 676–679.

Bando, Y., Katayama, T., Kasai, K., Taniguchi, M., Tamatani, M., Tohyama, M., 2003. GRP94 (94 kDa glucose-regulated protein) suppresses ischemic neuronal death against ischemia/reperfusion injury. Eur. J. Neurosci. 18, 829–840.

Bruijin, L.I., Miller, T.M., Cleveland, D.W., 2004. Unraveling the mechanism involved in motor neuron degeneration in ALS. Annu. Rev. Neurosci. 27, 723–749.

Brown Jr., R.H., Robberecht, W., 2001. Amyotrophic lateral sclerosis: pathogenesis. Semin. Neurol. 21, 131–139.

Cleveland, D.W., Rothstein, J.D., 2001. Deciphering selective motor neuron death in ALS. In: From Charcot to Lou Gehrig. Nat. Rev. Neurosci. 2, 806–819.

Filimonenko, M., Stuffers, S., Raiborg, C., Yamamoto, A., Malerød, L., Fisher, E.M., Isaacs, A., Brech, A., Stenmark, H., Simonsen, A., 2007. Functional multivesicular bodies are required for autophagic clearance of protein aggregates associated with neurodegenerative disease. J. Cell Biol. 179, 485–500.

Fischer, H., Koenig, U., Eckhart, L., Tschachler, E., 2002. Human caspase-12 acquired deleterious mutations. Biochem. Biophys. Res. Commun. 293, 722–726.

Gurney, M.E., 2000. What transgenic mice tell us about neurodegenerative disease. Bioessays 22, 297–304.

Hitomi, J., Katayama, T., Eguchi, Y., Kudo, T., Taniguchi, M., Koyama, Y., Manabe, T., Yamagishi, S., Bando, Y., Imaizumi, K., Tsujimoto, Y., Tohyama, M., 2004. Involvement of caspase-4 in endoplasmic reticulum stress-induced apoptosis and Aβ-induced cell death. J. Cell Biol. 165, 347–356.

Hyun, D.H., Lee, M., Halliwell, B., Jenner, P., et al., 2003. Proteasomal inhibition causes the formation of protein aggregates containing a wide range of proteins, including nitrated proteins. J. Neurochem. 86, 363–373.

Ilieva, E.V., Ayala, V., Jové, M., Dalfó, E., Cacabelos, D., Povedano, M., Bellmunt, M.J., Ferrer, I., Pamplona, R., Portero-Otín, M., 2007. Oxidative and endoplasmic reticulum stress interplay in sporadic amyotrophic lateral sclerosis. Brain 130, 3111–3123.

Johnston, J.A., Dalton, M.J., Gurney, M.E., Kopito, R.R., 2000. Formation of high molecular weight complexes of mutant Cu, Zn-superoxide dismutase in a mouse model for familial amyotrophic lateral sclerosis. Proc. Natl. Acad. Sci. U. S. A. 97, 12571–12576.

Julien, J.P., 2001. Amyotrophic lateral sclerosis. Unfolding the toxicity of the misfold. Cell 104, 581–591.

Kanekura, K., Nishimoto, I., Aiso, S., Matsuoka, M., 2006. Characterization of amyotrophic lateral sclerosis-linked P56S mutation of vesicle-associated membrane protein-associated protein B (VAPB/ALS8). J. Biol. Chem. 281, 30223–30233.

Kanekura, K., Suzuki, H., Aiso, S., Matsuoka, M., 2009. ER stress and unfolded protein response in amyotrophic lateral sclerosis. Mol. Neurobiol. 39, 81–89.

Katayama, T., Imaizumi, K., Sato, N., Miyoshi, K., Kudo, T., Hitomi, J., Morihara, T., Yoneda, T., Gomi, F., Mori, Y., Nakano, Y., Takeda, J., Tsuda, T., Itoyama, Y., Murayama, O., Takashima, A., St. George-Hyslop, P., Takeda, M., Tohyama, M., 1999. Presenilin-1 mutations downregulate the signalling pathway of the unfolded protein response. Nat. Cell Biol. 1, 479–485.

Kato, S., Horiuchi, S., Liu, J., Cleveland, D.W., Shibata, N., Nakashima, K., Nagai, R., Hirano, A., Takikawa, M., Kato, M., Nakano, I., Ohama, E., 2000. Advanced glycation endproduct-modified superoxide dismutase-1 (SOD1)-positive inclusions are common to familial amyotrophic lateral sclerosis patients with SOD1 gene mutations and transgenic mice expressing human SOD1 with a G85R mutation. Acta Neuropathol. 100, 490–505.

Kikuchi, H., Almer, G., Yamashita, S., Guegan, C., Nagai, M., et al., 2006. Spinal cord endoplasmic reticulum stress associated with a microsomal accumulation of mutant superoxide dismutase-1 in an ALS model. Proc. Natl. Acad. Sci. U. S. A. 103, 6025–6030.

Kouroku, Y., Fujita, E., Jimbo, A., Kikuchi, T., Yamagata, T., Momoi, M.Y., Kominami, E., Kuida, K., Sakamaki, S., Yonehara, S., Momoi, T., 2002. Polyglutamine aggregates stimulate ER stress signal and caspase-1 activation. Hum. Mol. Genet. 11, 1505–1515.

Mackenzie, I.R., Bigio, E.H., Ince, P.G., Geser, F., Neumann, M., Cairns, N.J., Kwong, L.K., Forman, M.S., Ravits, J., Stewart, H., Eisen, A., McClusky, L., Kretzschmar, H.A., Monoranu, C.M., Highley, J.R., Kirby, J., Siddique, T., Shaw, P.J., Lee, V.M., Trojanowski, J.Q., 2007. Pathological TDP-43 distinguishes sporadic amyotrophic lateral sclerosis from amyotrophic lateral sclerosis with SOD1 mutations. Ann. Neurol. 61, 427–434.

Nakagawa, T., Zhu, H., Morishima, N., Li, E., Xu, J., Yankner, B.A., Yuan, J., 2000. Caspase-12 mediates endoplasmic reticulum-specific apoptosis and cytotoxicity by amyloid-beta. Nature 403, 98–103.

Nishimura, A.L., Mitne-Neto, M., Silva, H.C., Richieri-Costa, A., Middleton, S., Cascio, D., Kok, F., Oliveira, J.R., Gillingwater, T., Webb, J., Skehel, P., Zatz, M., 2004. A mutation in the vesicle-trafficking protein VAPB causes late-onset spinal muscular atrophy and amyotrophic lateral sclerosis. Am. J. Hum. Genet. 75, 822–831.

Okado-Matsumoto, A., Fridovich, I., 2001. Subcellular distribution of superoxide dismutases (SOD) in rat liver: Cu, Zn-SOD in mitochondria. J. Biol. Chem. 276, 38388–38393.

Rosen, D.R., Siddique, T., Patterson, D., Figlewicz, D.A., Sapp, P., et al., 1993. Mutations in Cu/Zn superoxide dismutase gene are associated with familial amyotrophic lateral sclerosis. Nature 362, 59–62.

Rowland, L.P., Schneider, N.A., 2001. Amyotrophic lateral sclerosis. N. Engl. J. Med. 344, 1688–1700.

Ryu, E.J., Harding, H.P., Angelastro, J.M., Vitolo, O.V., Ron, D., Greene, L.A., 2002. Endoplasmic reticulum stress and the unfolded protein response in cellular models of Parkinson's disease. J. Neurosci. 22, 10690–10698.

Sato, N., Imaizumi, K., Manabe, M., Taniguchi, M., Hitomi, J., Katayama, T., Yoneda, T., Morihara, T., Yasuda, Y., Takagi, T., Kudo, T., Tsuda, T., Itoyama, Y., Mukifuchi, T., Fraser, P.E., St. George-Hyslop, P., Tohyama, M., 2001. Increased production of beta-amyloid and vulnerability to endoplasmic reticulum stress by an aberrant spliced form of presenilin 2. J. Biol. Chem. 276, 2108–2114.

Schagger, H., 2006. Tricine–SDS-PAGE. Nat. Protoc. 1, 16–22.

Sturtz, L.A., Diekert, K., Jensen, L.T., Lill, R., Culotta, V.C., 2001. A fraction of yeast Cu, Zn-superoxide dismutase and its metallochaperone, CCS, localize to the intermembrane space of mitochondria. A physiological role for SOD1 in guarding against mitochondrial oxidative damage. J. Biol. Chem. 276, 38084–38089.

Tobisawa, S., Hozumi, Y., Arawaka, S., Koyama, S., Wada, M., Nagai, M., Aoki, M., Itoyama, Y., Goto, K., Kato, T., 2003. Mutant SOD1 linked to familial amyotrophic lateral sclerosis, but not wild-type SOD1, induces ER stress in COS7 cells and transgenic mice. Biochem. Biophys. Res. Commun. 303, 496–503.

Wate, R., Ito, H., Zhang, J.H., Ohnishi, S., Nakano, S., Kusaka, H., 2005. Expression of an endoplasmic reticulum-resident chaperone, glucose-regulated stress protein 78, in the spinal cord of a mouse model of amyotrophic lateral sclerosis. Acta Neuropathol. 110 (6), 557–562.

Wittig, I., Braun, H.-P., Schagger, H., 2006. Blue native PAGE. Nat. Protoc. 1, 418–428.

Wootz, H., Hansson, I., Korhonen, L., Napankangas, U., Lindholm, D., 2004. Caspase-12 cleavage and increased oxidative stress during motoneuron degeneration in transgenic mouse model of ALS. Biochem. Biophys. Res. Commun. 322, 281–286.

Yamagishi, S., Koyama, Y., Katayama, T., Taniguchi, M., Hitomi, J., Kato, M., Aoki, M., Itoyama, Y., Tohyama, N., 2007. An in vitro model for Lewy body hyaline inclusion/Astrocytic hyaline inclusion: induction by ER stress with an ALS-linked SOD1 mutation. PloS One 10, 130–140.

Yukioka, F., Matsuzaki, S., Kawamoto, K., Koyama, Y., Hitomi, J., Katayama, T., Tohyama, M., 2008. Presenilin-1 mutation activates the signaling pathway of caspase-4 in endoplasmic reticulum stress-induced apoptosis. Neurochem. Int. 52, 683–687.

Please cite this article in press as: Koyama, Y., et al., Familiar amyotrophic lateral sclerosis (FALS)-linked SOD1 mutation accelerates neuronal cell death by activating cleavage of caspase-4 under ER stress in an *in vitro* model of FALS. Neurochem. Int. (2010), doi:10.1016/j.neuint.2010.08.023

FEBS Letters 582 (2008) 3693–3700

N-terminal region of α-synuclein is essential for the fatty acid-induced oligomerization of the molecules

Hiroki Karube[1], Masahiro Sakamoto[1], Shigeki Arawaka*, Susumu Hara, Hiroyasu Sato, Chang-Hong Ren, Saori Goto, Shingo Koyama, Manabu Wada, Toru Kawanami, Keiji Kurita, Takeo Kato

Department of Neurology, Hematology, Metabolism, Endocrinology and Diabetology, Faculty of Medicine, Yamagata University, 2-2-2 Iida-Nishi, Yamagata 990-9585, Japan

Received 18 September 2008; revised 30 September 2008; accepted 2 October 2008

Available online 9 October 2008

Edited by Barry Halliwell

Abstract Exposure of α-synuclein (αS), a major component of Lewy bodies in Parkinson's disease, to polyunsaturated fatty acids (PUFAs) triggers the formation of soluble αS oligomers. Here, we demonstrate that PUFA binds recombinant αS protein through its N-terminal region (residues 2–60). In HEK293 cells, αS mutants lacking the N-terminal region failed to form oligomers in the presence of PUFA. The PUFA-induced αS oligomerization was accelerated by C-terminal truncation or Ser129 phosphorylation of αS; however, this effect was abolished by deletion of the N-terminus. The results indicate that the N-terminus of αS is essential for the PUFA-induced αS oligomerization.

Keywords: Parkinson's disease; α-Synuclein; Oligomerization; Fatty acid; Truncation; Phosphorylation

1. Introduction

Parkinson's disease (PD) is characterized by the progressive degeneration of dopaminergic neurons in the substantia nigra and the presence of intracytoplasmic filamentous inclusions called Lewy bodies (LBs) and Lewy neurites (LNs). Identification of missense mutations in the α-Synuclein (αS) gene (A30P, A53T, and E46K) [1–3] and the multiplication [4] of the locus in autosomal-dominant familial PD indicates a direct link of αS to the pathogenesis of familial PD. αS is also thought to play a critical role in sporadic cases of PD, because fibrillized αS is a major component of LBs and LNs [5]. In vitro experiments have shown that αS readily oligomerizes into fibrils that share ultrastructural features of fibrils in LBs [6]. Furthermore, overexpression of human wild-type [7] or A53T [8,9] αS in transgenic mice results in motor impairment with the development of αS inclusions. Feany and colleagues have also reported that overexpression of wild-type, A30P or A53T-αS in *Drosophila* shows loss of dopaminergic neurons with an increase in filamentous αS inclusions [10]. Accumulated evidence suggests that the oligomerization of αS into fibrils affects the toxicity of the molecule [11]. Previous studies have demonstrated that the oligomerization of αS is accelerated by oxidation and nitration of αS [12], phosphorylation of αS at Ser129 [13,14], C-terminal truncation of αS [15] or binding of phospholipids to αS [16]. However, the exact biochemical mechanisms for the formation of pathological αS oligomers remain to be elucidated.

Sharon et al. reported that the N-terminus (residues 2–19) and the C-terminus (residues 123–140) of αS have homology to the fatty acid (FA)-binding motif of fatty acid-binding protein (FABP) [17]. They also showed that recombinant αS directly binds to FA in a stochiometric manner, and that soluble, lipid-associated monomers and oligomers of αS are present in transgenic mouse brains expressing wild-type or A53T-αS [17,18]. On the basis of the facts, they concluded that αS has the properties of FABP [17,18]. They further demonstrated that exposure of monomeric αS to polyunsaturated fatty acids (PUFAs) promotes the formation of soluble αS oligomers in cultured mesencephalic cells [18]. In the brains of PD and dementia with Lewy bodies, the amount of soluble, lipid-associated αS oligomers increased [18]. Since the soluble αS oligomers seem to be precursors of fibrils [11], the findings suggest that the binding of αS to PUFA is one of the key events in the process for conversion from soluble monomers to pathological oligomers of αS.

The present study was carried out to determine the αS region responsible for the binding to FA by using a series of αS deletion mutants, and to assess a role of the binding of αS to PUFA in the oligomerization of αS. The results show that the binding of αS to PUFA in its N-terminal region is essential for the PUFA-induced oligomerization of αS.

2. Materials and methods

2.1. Plasmid construction

Wild-type human αS (Wt-αS) cDNA and human G protein-coupled receptor kinase 5 (GRK5) cDNA were cloned into the pcDNA3.1 vector (Invitrogen) [14]. αS deletion mutant cDNAs and αS familial PD-linked mutant (A30T, E46K and A53T) cDNAs were generated by the two-step PCR mutagenesis method. Nucleotide sequences of all constructs were confirmed.

*Corresponding author. Fax: +81 23 628 5318.
E-mail address: arawaka@med.id.yamagata-u.ac.jp (S. Arawaka).

[1]These authors contributed equally to this work.

Abbreviations: PD, Parkinson's disease; αS, alpha-synuclein; LB, Lewy body; LN, Lewy neurite; FA, fatty acid; PUFA, polyunsaturated fatty acid; FABP, fatty acid-binding protein; OA, Oleic acid; ALA, α-linolenic acid; GRK, G protein-coupled receptor kinase; NAC, non-amyloid β-protein component

0014-5793/$34.00
doi:10.1016/j.febslet.2008.10.001